NASA CR - 165164

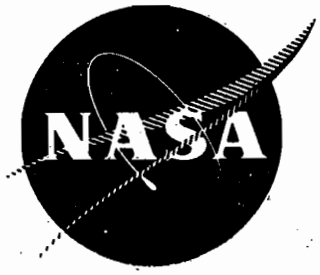

BAFFLE APERTURE DESIGN STUDY OF HOLLOW CATHODE EQUIPPED ION THRUSTERS

PREPARED FOR

LEWIS RESEARCH CENTER

NATIONAL AERONAUTICS AND SPACE ADMINSTRATION

GRANT NGR-06-002-112

by

John R. Brophy

Approved by

Paul J. Wilbur

October 1980

Department of Mechanical Engineering
Colorado State University
Fort Collins, Colorado

1. Report No.	2. Government Accession No.	3. Recipient's Catalog No.
NASA CR-165164		

4. Title and Subtitle	5. Report Date
BAFFLE APERTURE DESIGN STUDY OF HOLLOW CATHODE EQUIPPED ION THRUSTERS	Oct. 1980
	6. Performing Organization Code
7. Author(s) John R. Brophy and Paul J. Wilbur	8. Performing Organization Report No.
	10. Work Unit No.
9. Performing Organization Name and Address Department of Mechanical Engineering Colorado State University Fort Collins, Colorado 80523	11. Contract or Grant No. NGR-06-002-112
	13. Type of Report and Period Covered Dec. 1, 1979 - Oct. 1, 1980
12. Sponsoring Agency Name and Address National Aeronautics and Space Administration Washington, D. C. 20546	14. Sponsoring Agency Code

15. Supplementary Notes Grant Monitor - William Kerslake, NASA Lewis Research Center, Cleveland, Ohio 44135. This report is a reproduction of the Master's Thesis of John R. Brophy. It is submitted to the sponsor and to the distribution list in this form both as a presentation of the technical material, and as an indication of the academic program supported by the grant.

16. Abstract

A simple theoretical model which can be used as an aid in the design of the baffle aperture region of a hollow cathode equipped ion thruster is developed. An analysis of the ion and electron currents in both the main and cathode discharge chambers is also presented. From this analysis a model of current flow through the aperture, which is required as an input to the design model, is developed. This model is verified experimentally. The dominant force driving electrons through the aperture is shown to be the force due to the electrical potential gradient. The diffusion process is modeled according to the Bohm diffusion theory. A number of simplifications are made to limit the amount of detailed plasma information required as input to the model to facilitate the use of the model in thruster design. This simplified model is shown to give remarkably consistant results with experimental results obtained with a given thruster geometry over substantial changes in operating conditions. The model does, however, appear to be uncertain to about a factor of two for different thruster cathode region geometries. The design usefulness is limited by this factor of two uncertainty and by the accuracy to which the plasma parameters required as inputs to the model can be specified.

17. Key Words (Suggested by Author(s))	18. Distribution Statement
Electrostatic Thruster Hollow Cathode Electron Diffusion	Unclassified - Unlimited

19. Security Classif. (of this report)	20. Security Classif. (of this page)	21. No. of Pages	22. Price*
Unclassified	Unclassified	77	

* For sale by the National Technical Information Service, Springfield, Virginia 22161

TABLE OF CONTENTS

LIST OF FIGURES

Table of Figures (Cont.) Page

NOMENCLATURE

A	Area (m^2)
B	Magnetic Field (tesla)
D	Diffusion Coefficient (m^2/s)
E	Electric Field (v/m)
e	Electronic Charge (1.6×10^{-19} coul.)
I	Current (A)
i	Unit Vector
j	Current Density (A/m^2)
k	Boltzmann's Constant (1.38×10^{-23} J/°K)
m	Mass (kg)
n	Particle Density (m^{-3})
P	Electron Pressure (N/m^2)
Q	Collision Cross Section (m^2)
r	Radial Position (m)
T	Temperature (°K)
V	Plasma Potential (volts)
v	Fluid velocity (m/s)
w	Average Random Particle Velocity (m/s)
Γ	Particle Flux $(m^2 s)^{-1}$
z	Axial Position (m)
ε	Electron Energy (J)
Λ	Non-Dimensionalized Plasma Shielding Distance
ν	Collision Frequency (Hz)
ω	Cyclotron Frequency (Rad/s)

SUBSCRIPTS

A	Pertaining to the Anode
a	Pertaining to the Baffle Aperture
B	Bohm Diffusion
b	Extracted Ion Beam
C	Classical Diffusion
c	Cathode Region
D	Pertaining to the Discharge
E	Pertaining to the Cathode Emission
exp	Experiment
e	Electron
g	Pertaining to the Center of the Aperture Gap
i	Ion
k	Pertaining to the Keeper Electrode
m	Main Discharge Region
n	Neutral Atom
P	Production
p	Pertaining to the Primary Electrons
s	Pertaining to the Screen Grid
w	Pertaining to Cathode Potential Surfaces
θ	Azimuthal Direction
$\perp$	Direction Normal to Magnetic Field Lines
$\parallel$	Direction Parallel to Magnetic Field Lines

SUPERSCRIPTS

$\bar{}$	Average Quantity
*	Non-dimensional Quantity

I. INTRODUCTION

In the past the design and optimization of ion thrusters has been accomplished primarily by the cut and try method.[1-6] That is, a systematic variation of the parameters that influence thruster operation was performed until an acceptable configuration was obtained. This procedure is both costly and time consuming. Consequently, there is a need for the development of analytical models which relate various aspects of thruster operation to, a priori, specifiable thruster parameters. The present investigation is an attempt at the development of a model which deals with the creation of high energy electrons within the discharge chamber of a hollow cathode equipped ion thruster.

After presenting a brief qualitative description of the operation of electron bombardment ion thrusters, the reasons for the use of hollow cathodes as well as the special considerations required by their use will be given. Next, the development of the theoretical model and the assumptions used in its derivation is presented. Finally, a comparison of the model with experimental data will be given for a wide variety of thruster operating conditions and two different discharge chamber geometries.

The plasma properties and operating parameters given are representative of mercury which was the propellant used in this investigation. Units will be SI unless otherwise stated.

II. THRUSTER OPERATION

Electron Bombardment Thrusters

An electron bombardment ion thruster typically consists of a cylindrical discharge chamber bounded on the sides by an anode, on the upstream end by the body, and on the downstream end by the accelerator system as suggested by Fig. 1. An electron emitter or cathode is located inside the thruster and a plasma discharge is sustained between the cathode and an electron collector or anode which is typically biased 30 to 40 volts positive of the cathode. The accelerator system consists of a set of multi-aperture electrode plates called grids. The inner electrode is called the screen grid and is usually maintained at a high positive potential, as is the thruster body. The outer electrode is biased strongly negative of the screen grid and is called the accelerator grid. A strong electric field exists between the grids which accelerates the ions produced in the plasma to provide the thrust.

During operation neutral propellant gas is injected into the thruster at the upstream end of the discharge chamber. The cathode which is heated to incandescence emits a stream of electrons. Since the cathode is maintained 30 to 40 volts negative of the anode these electrons are accelerated into the main discharge region. Electrons which have undergone this acceleration are called primary electrons. The energy of these primary electrons is sufficient to assure that the associated ionization cross section is near a maximum for the given propellant. A second group of electrons originates from the inelastic interaction of the primaries with the ions and neutral propellant atoms. These interactions reduce the energy of the primary electrons and release low energy secondary electrons to form an electron

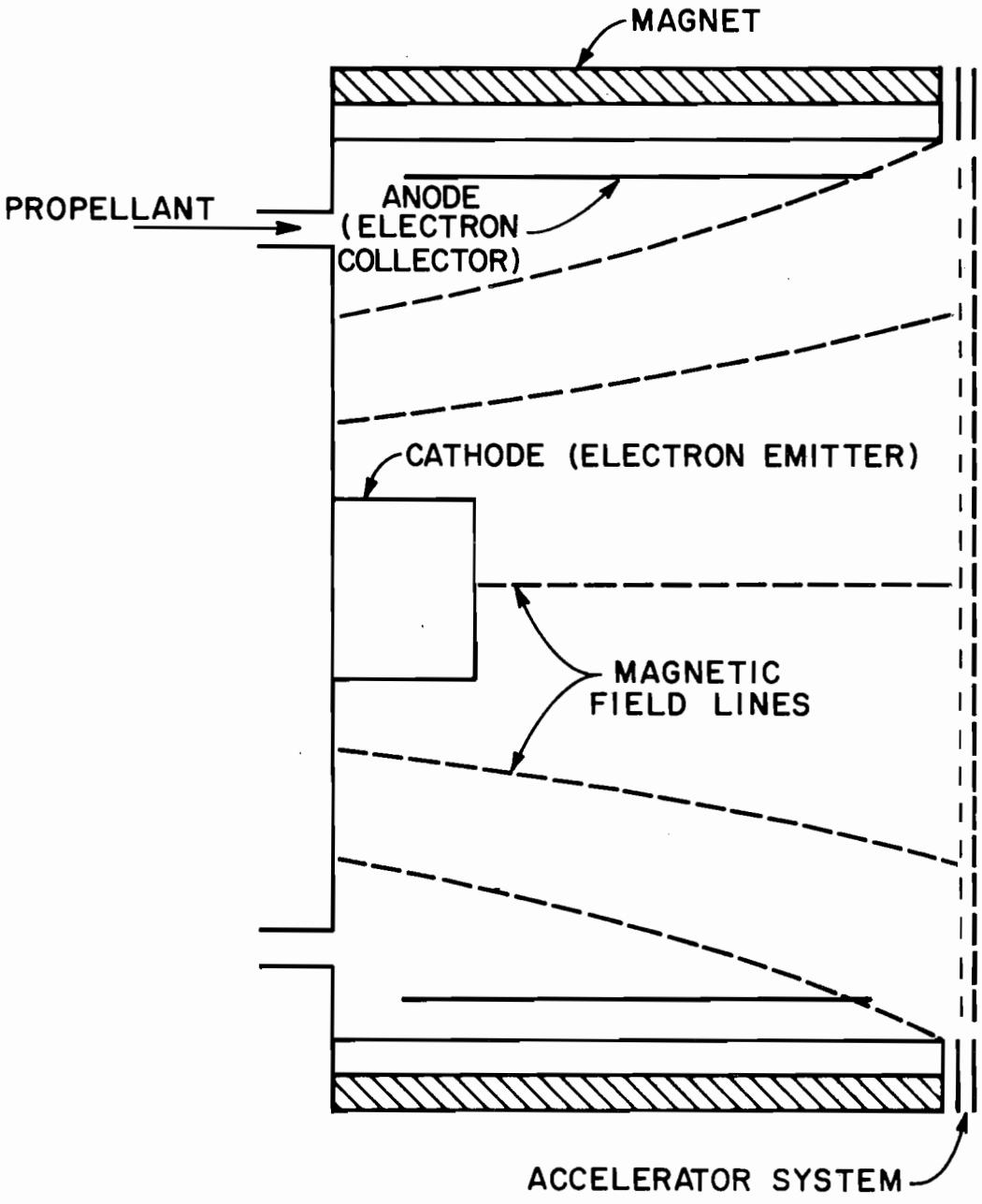

Fig. 1 Electron Bombardment Ion Thruster

population with a nearly Maxwellian energy distribution. The Maxwellian group typically contains 90-95 percent of the plasma electrons yet only accounts for roughly half of the ionizations.[7] It is possible for both electron populations to exist simultaneously in the discharge chamber due to the low interaction rate between the primary and Maxwellian electrons.[8]

Since the mean free path for electron-neutral ionization collisions is on the order of meters while typical discharge chamber dimensions are on the order of several centimeters a magnetic field is employed to prevent the primary electrons from having direct access to the anode. The strength of the magnetic field is determined by the need to contain the primary electrons while at the same time allowing the Maxwellian electrons to diffuse to the anode at a rate sufficient to sustain the discharge. The configuration and strength of this magnetic field has a significant effect on the operation of this type of thruster and consequently has been the subject of numerous studies.[1-4, 9-12]

The plasma produced within the discharge chamber will typically assume a potential slightly positive of the anode.[13] Consequently a potential sheath will exist at all plasma boundaries. The magnitude of this sheath at cathode potential surfaces depends on the magnitude of the discharge voltage applied between the cathode and the anode, and is typically 30 to 40 volts. This sheath potential is sufficient to reflect all but the most energetic electrons in the tail of the Maxwellian distribution.[7] At the anode, however, there is a significant probability that most electrons will be collected since the plasma potential is within a few volts of the anode potential. Consequently, the vast majority of electrons can only leave the discharge chamber at anode potential surfaces.

The ions produced within the plasma move with nearly equal probability in all directions. Those that fall on solid thruster surfaces recombine with electrons and are vaporized back into the discharge chamber as neutral atoms.[7] Those that reach the downstream end of the thruster are extracted out through the accelerator system to form the beam current.

Electron Sources

Steady state thruster operation requires that high energy electrons be continuously supplied to the main discharge chamber to sustain the discharge while low energy electrons are continuously removed by the anode. Early ion thruster designs used refractory metal filaments as the source of primary electrons.[14] These filaments, typically made of tantalum or tungsten, emit electrons when heated to sufficiently high temperatures. The emitted electrons are then accelerated across the cathode potential sheath which surrounds the filament into the main discharge chamber to become primary electrons. Since the potential sheath is electrostatic in nature,[15] the acceleration of the electrons from the cathode filament is also an electrostatic process, and the primary electrons enter the main discharge region with a nearly monoenergetic energy distribution. This type of cathode however proved unsuitable for space applications due to its high specific heating power characteristic (670 W/A) and short lifetime ($\sim$100 hours).[14] In order to reduce the specific heating power, various cathode designs utilizing oxide coatings have been investigated. The oxide coating serves to reduce the work function of the emitter allowing it to operate at lower temperatures and hence lower specific heating powers. While the specific heating power was generally low enough for most oxide

cathodes they had the disadvantage that exposure to air caused chemical deactivation of the oxide which prevented them from being preflight tested in a flight qualified system.[14]

The hollow cathode has replaced both refractory metal and oxide cathodes as the source of electrons in ion thrusters for space applications for the following reasons. First, they can be operated at specific heating powers of less than 40 W/A.[14] Second, they exhibit very long lifetimes,[1,16] (lifetimes in excess of 10,000 hours have been achieved).[14] This is necessary since the low-thrust nature of electron bombardment thrusters requires long mission times to achieve the desired spacecraft velocity increment. Finally, a hollow cathode can be restarted a number of times even after exposure to air, allowing it to be preflight tested.[1, 14,16]

Hollow Cathode Equipped Thruster Operation

A typical hollow cathode equipped ion thruster is shown schematically in Fig. 2. The use of a hollow cathode generally requires the addition of a small loop anode called a keeper located downstream of the cathode. This keeper electrode draws sufficient electron current to maintain the cathode discharge in the presence of low emission conditions and plasma fluctuations. When heated to sufficiently high temperatures the hollow cathode will emit a stream of electrons. These electrons flow out of a small orifice at the downstream end of the cathode and into a small subchamber called the cathode discharge region. This region is separated from the main discharge chamber through the use of a baffle plate. The plasma potential in the cathode discharge region will typically assume a potential slightly positive of the keeper electrode. Therefore, biasing the keeper positive of the cathode

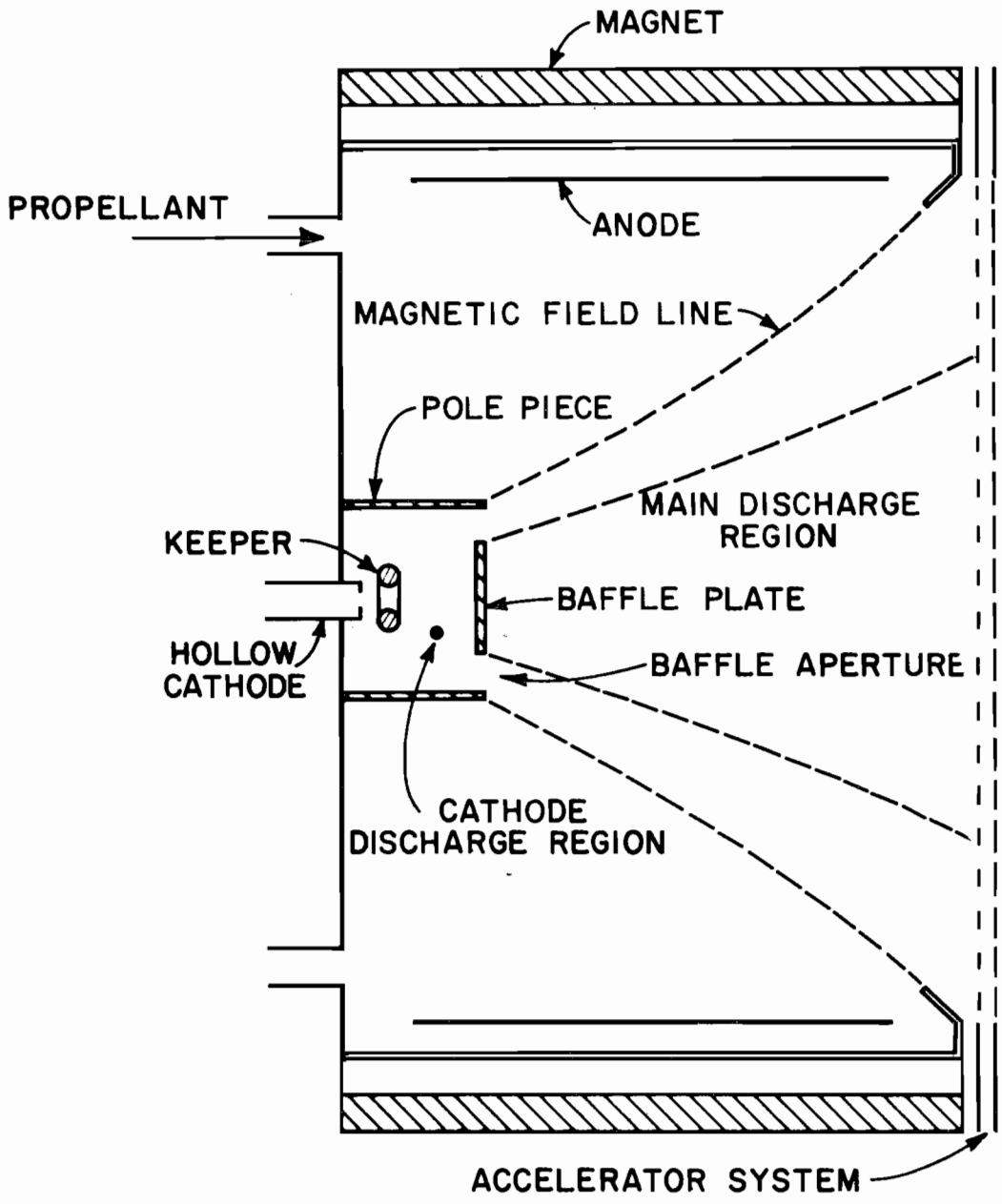

Fig. 2 Hollow Cathode Equipped Electron Bombardment Ion Thruster

will create a favorable potential sheath near the cathode orifice which facilitates the extraction of electrons from the cathode. The plasma potential of the cathode discharge region is generally about 10 volts positive of the cathode itself. Since the boundaries of this region are maintained at cathode potential a potential sheath will exist at each of these surfaces. The magnitude of this sheath is sufficient to reflect nearly every electron incident upon it. The cathode chamber connects to the main discharge chamber via an annular opening called the baffle aperture. Because the sheath potentials in the cathode discharge region prevent the electrons from reaching the cathode chamber walls, electrons may only leave this region either by being collected by the keeper electrode or by diffusing through the baffle aperture.

Cathode Discharge Region Current Balance

Fig. 3 indicates the currents of electrons and ions into and out of the cathode discharge region of a normally operating thruster, The arrows for both ions and electrons point in the direction of actual particle motion. Consequently, for the electrons the arrows point in the direction opposite to that of conventional current flow while for the ions they point in the conventional current flow direction. Under steady state operating conditions the net rate at which electrons enter the cathode discharge region must be equal to the net rate at which ions enter, that is,

$$\underbrace{I_{e_E} + I_{e_P}}_{\text{Electrons Entering}} - \underbrace{I_{e_a} - I_{e_w} - I_{e_k}}_{\text{Electrons Leaving}} = \underbrace{I_{i_p} + I_{i_a}}_{\text{Ions Entering}} - \underbrace{I_{i_w}}_{\text{Ions Leaving}} . \qquad (1)$$

As stated above the electron current to the walls (I_{e_w}) may be neglected. In addition the ion current which enters through the baffle

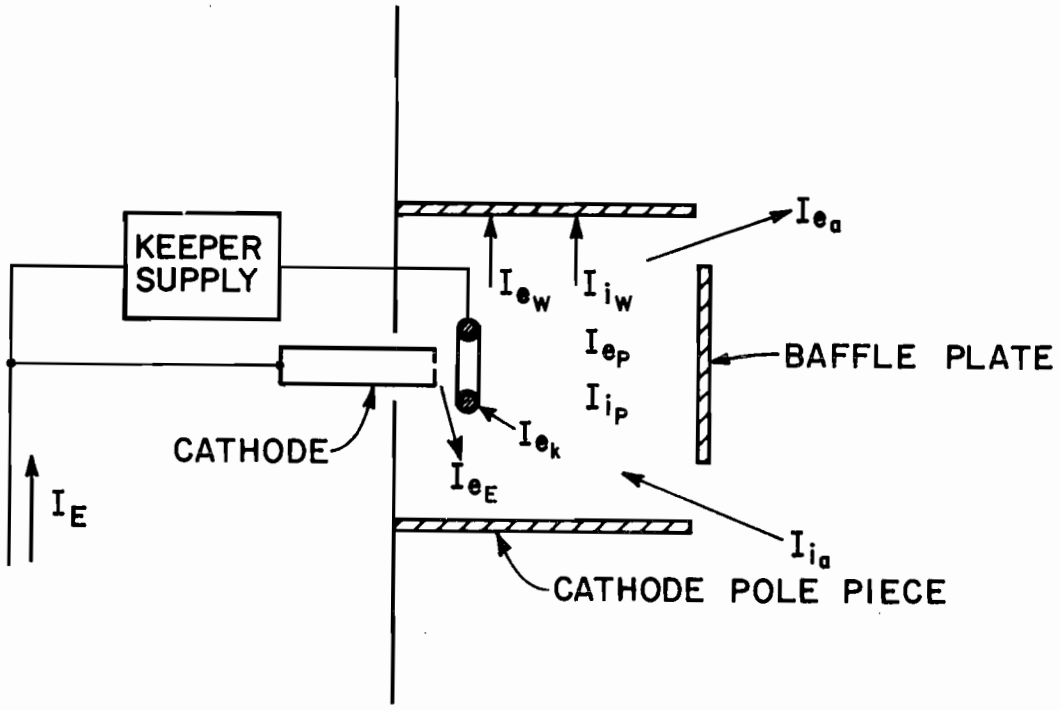

Electrons

I_{e_E} = Cathode Electron Emission Current

I_{e_a} = Baffle Aperture Electron Current

I_{e_w} = Electron Current to Cathode Potential Surfaces

I_{e_k} = Keeper Electron Current

I_E = Net Cathode Emission Current, $I_E = I_{e_E} - I_{e_k}$

I_{e_p} = Electron Production Rate

Ions

I_{i_a} = Baffle Aperture Ion Current

I_{i_p} = Ion Production Rate

I_{i_w} = Ion Current to Cathode Region Walls

Fig. 3 Electron and Ion Currents in Cathode Discharge Chamber

aperture is negligible primarily as a result of the small area of the aperture.* Further, the production rate of ions (I_{i_p}) and of electrons (I_{e_p}) in this region through ionizations must be equal, therefore Eq. (1) may be written in the form,

$$I_{e_a} = I_{e_E} - I_{e_k} + I_{i_w} \quad . \tag{2}$$

Defining the net cathode emission current (I_E) as the electron current which is emitted by the cathode and not subsequently collected by the keeper, i.e. as,

$$I_E = I_{e_E} - I_{e_k} \tag{3}$$

Eq. (2) can be written,

$$I_{e_a} = I_E + I_{i_w} \quad . \tag{4}$$

In addition, the calculations presented in Appendix A based on measured cathode region plasma densities indicate that the ion current to the cathode chamber walls (I_{i_w}) is small compared to the net emission current (I_E). Thus Eq. (4) may be written in the form,

$$I_{e_a} \approx I_E \quad . \tag{5}$$

That is, the magnitude of the electron current through the baffle aperture into the main discharge region is approximately equal to the net cathode emission current.

The cathode discharge region electrons are driven through the baffle aperture under the influence of a density gradient force and a

---

* Typical ion currents through the aperture are on the order of 0.05 amps, and are less generally than 2% of the electron current through the aperature. See Appendix A.

potential gradient force. The density gradient arises because the hollow cathode creates a cathode region plasma density which is generally greater than the density of the main discharge region. The potential gradient occurs as a result of the anode being biased positive of the cathode. A magnetic field oriented across the aperture is required to control the impedence of the baffle aperture region,[3,4,6,17-21]

This creates the following self consistant situation. The anode, being maintained at a potential positive of the cathode, draws the electrons emitted by the cathode through the baffle aperture into the main discharge region. The magnetic field oriented across the aperture creates an impedence to this flow of electrons, and thereby establishes the potential and density gradients in the vicinity of the baffle aperture. These potential and density gradients then serve to drive the electron current across the magnetic field and into the main discharge region. Hollow cathode equipped ion thrusters typically operate with a potential increase of about 30 volts through the baffle aperture. Electrons diffusing through the aperture region thus acquire an energy of approximately 30 electron volts and subsequently are referred to as primary electrons. In this case, however, the accelerating potential sheath is electromagnetic in nature,[17] not electrostatic as it was for the refractory metal and oxide cathodes. These primary electrons now have sufficient energies to ionize the neutral propellant atoms.

Main Discharge Region Current Balance

Electrons may enter the main discharge region either by coming through the baffle aperture or through the liberation of electrons in the ionization process. In both cases the electrons, as stated previously, are constrained by the plasma boundary potential sheaths to

leave the main discharge region only at the anode. The ions on the other hand only enter the main discharge region through ionizations. They may, however, leave this region by going through the baffle aperture, recombining on a cathode potential surface, recombining on an anode potential surface or being extracted into the ion beam by the accelerator system. Again for a steady state operating condition the net influx of electrons must be equal to the net influx of ions. With the help of Fig. 4, where the arrow convention is the same as that used in Fig. 3, the following equation can be written,

$$\underbrace{I_{e_a}}_{\text{Electrons Entering}} + I_{e_P} - \underbrace{I_{e_w} - I_{e_A}}_{\text{Electrons Leaving}} = \underbrace{I_{i_P}}_{\text{Ions Entering}} - \underbrace{I_{i_A} - I_{i_w} - I_{i_a} - I_{i_b}}_{\text{Ions Leaving}} . \tag{6}$$

Now since the electron current to cathode potential surfaces (I_{e_w}) and the ion current through the baffle aperture (I_{i_a}) are negligible and since the production rate of electrons (I_{e_P}) and of ions (I_{i_P}) through ionizations are approximately equal (neglecting double ion production) Eq. (6) can be written in the form,

$$I_{e_a} = I_{e_A} - I_{i_A} - I_{i_w} - I_{i_b} . \tag{7}$$

Because both electrons and ions are collected at the anode the discharge current, I_D, (i.e., the current through the anode power supply) is simply the difference between the electron and ion currents to the anode,

$$I_D = I_{e_A} - I_{i_A} . \tag{8}$$

Combining Eqs. (7) and (8) yields,

$$I_{e_a} = I_D - I_{i_w} - I_{i_b} . \tag{9}$$

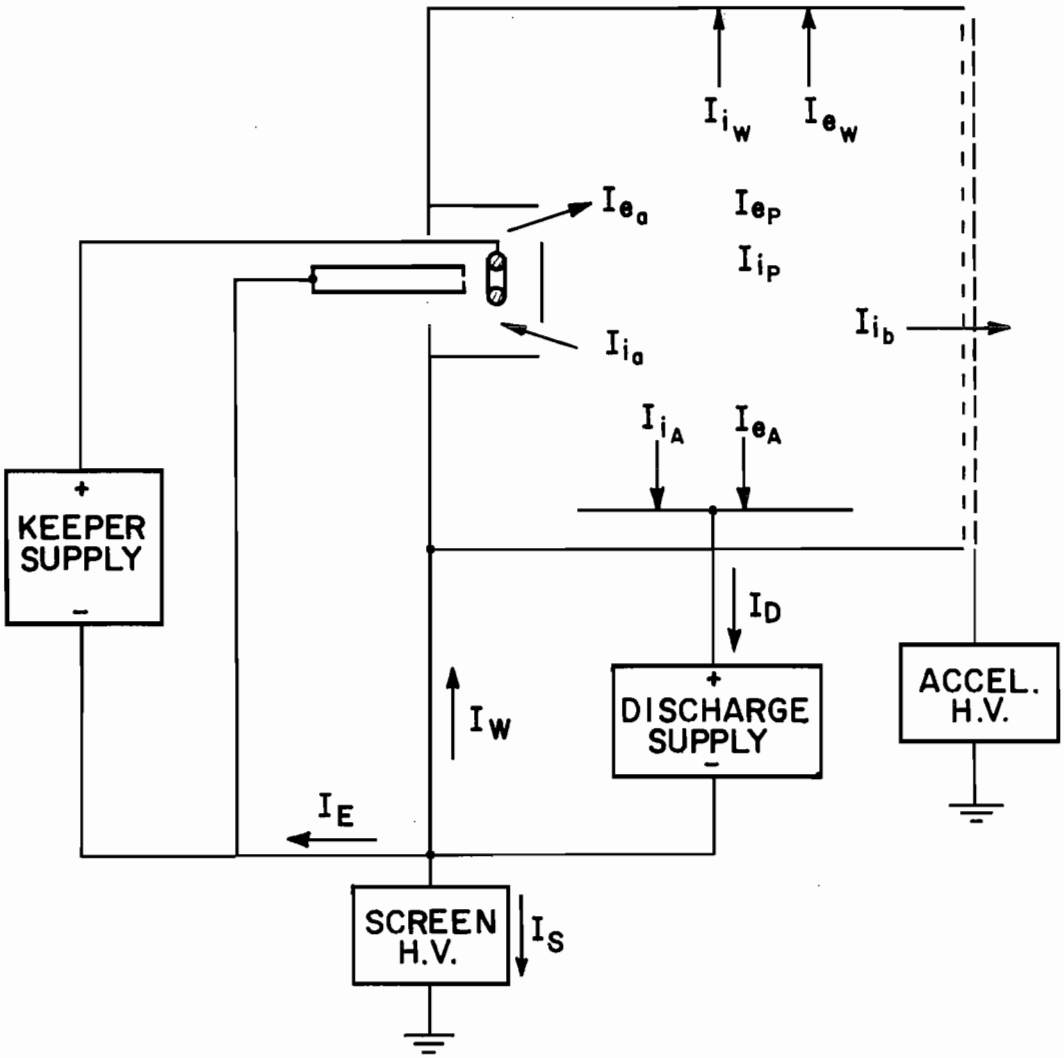

Electrons

- I_{e_a} = Baffle Aperture Electron Current
- I_{e_p} = Electron Production Rate
- I_{e_A} = Electron Current to the Anode
- I_{e_w} = Electron Current to Cathode Potential Surfaces
- I_D = Electron Current Through Discharge Supply
- I_S = Electron Current Through H.V. Screen Supply
- I_E = Net Cathode Emission Current

Ions

- I_{i_a} = Baffle Aperture Ion Current
- I_{i_p} = Ion Production Rate
- I_{i_A} = Ion Current to the Anode
- I_{i_w} = Ion Current to Cathode Potential surfaces
- I_{i_b} = Ion Beam Current

Fig. 4 Electron and Ion Currents in Main Discharge Chamber

Assuming the ions move with nearly equal probability in all directions the ion current to the cathode potential surfaces may be determined in terms of the beam current (I_{i_b}) by the relation,

$$I_{i_w} \approx \left(\frac{I_{i_b}}{A_s}\right) A_w \tag{10}$$

where A_s is the effective open area of the screen grid and A_w is the effective surface area of the ion production region* through which ions can flow to reach a cathode potential surface. Combining Eqs. (9) and (10) yields,

$$I_{e_a} \approx I_D - I_{i_b} \left(\frac{A_w + A_s}{A_s}\right) \quad . \tag{11}$$

By measuring the discharge current and beam current one should be able to approximate the current through the baffle aperture using this equation. Equation (11) thus provides an alternate method for approximating the baffle aperture current when it is not possible to measure the net cathode emission current directly.

Present Investigation

The present investigation is an attempt at the development of a theoretical model which relates, a priori, specifiable magnetic field, geometric and plasma parameters (density, potential, etc.) to the aperture impedence. It was not the intent of this investigation to determine the exact mechanism of the diffusion process of electrons through the aperture. Rather the simplest relation between the

---

* The ion production region is defined as the region of the main discharge chamber inside the virtual anode surface.[13]

electron current through the aperture and the forces acting on it, which agreed with experimental results, was sought. As stated previously, it is believed that the current is driven through the aperture across the magnetic field under the influence of both a plasma density gradient and a potential gradient. Thus any model describing the flow of electons in this region would be expected to require as inputs a description of these gradients. However, because a detailed knowledge of the plasma parameters in the aperture region is not generally known before a thruster is built and tested, it was considered desirable to require as inputs to the model a minimum of plasma parameters (density, potential, etc.). This condition was imposed on the model in order that the end result be at least reasonably easy to apply in the design phase of a thruster. Because it is essentially the difference in these plasma properties between the cathode and main discharge regions which drives the electrons through the aperture, it was felt that plasma property measurements to be used as inputs to the model could be limited to one position in the cathode region and one in the main discharge region.

The plasma density, potential and magnetic field variations through the aperture have all been discussed thus far as being important to the processes on going in the aperture region. In addition one might expect that the physical area of the aperture as well as the magnitude of the current through it might also be important. Thus a systematic variation of these quantities suggests itself as a means of testing the model.

III. THEORY

Development of Theoretical Model

The approach to the problem of developing a theory which relates the current through the baffle aperture to the geometry, magnetic field and plasma properties in this region was to treat the electron population as a fluid. Only those forces which act on fluid elements were considered; individual particle motions as well as ion motions were neglected. The fluid model is appropriate for the following reasons. First there are far too many particles involved to follow individual particle motions and second the magnetic field can play the role of collisions in the sense that it limits electron free streaming and forces the electrons to exhibit collective behavior.[22] For motions perpendicular to the magnetic field then, the fluid theory is a good approximation.[22] The fluid equation of motion for the electrons, known as the momentum transfer equation is written,[23]

$$m_e n \left[\frac{\partial \vec{v}}{\partial t} + (\vec{v} \cdot \vec{\nabla}) \vec{v} \right] = -ne(\vec{E} + \vec{v} \times \vec{B}) - \vec{\nabla} P - \nu n m_e \vec{v} \quad . \qquad (12)$$

This equation determines the average velocity of the system of particles under consideration and assumes that the pressure is locally isotropic. Assuming there is no net change in the average fluid velocity and for steady state conditions Eq. (12) becomes,

$$ne(\vec{E} + \vec{v} \times \vec{B}) + \vec{\nabla} P + \nu n m_e \vec{v} = 0 \quad . \qquad (13)$$

The current density, $\vec{j}$, is introduced through the equation,

$$\vec{j} = -ne\vec{v} \qquad (14)$$

and using the definition of plasma potential in terms of the electric field, $\vec{\nabla} V = -\vec{E}$, Eq. (13) can be written as,

$$ne\left(\vec{\nabla}V + \frac{\vec{j} \times \vec{B}}{ne}\right) - \vec{\nabla}P + \frac{\nu n m_e}{e}\vec{j} = 0 \qquad (15)$$

At this point it is appropriate to specify the coordinate system to be used. The coordinate system is chosen such that the axes are everywhere parallel or perpendicular to the magnetic field lines. This is illustrated in the cathode pole piece shown in Fig. 5. In this coordinate system the current density can be written as,

$$\vec{j} = j_\perp \vec{i}_\perp + j_\theta \vec{i}_\theta + j_{\parallel} \vec{i}_{\parallel} \qquad (16)$$

and the magnetic field as,

$$\vec{B} = B \vec{i}_{\parallel} \qquad (17)$$

where $\vec{i}_\perp$, $\vec{i}_\theta$ and $\vec{i}_{\parallel}$ are unit vectors in the perpendicular, azimuthal and parallel directions respectively. Writing Eq. (15) in component form yields,

$$\text{Normal to B} \quad : ne\nabla_\perp V - \nabla_\perp P + j_\theta B + \frac{m_e \nu}{e} j_\perp = 0 \qquad (18)$$

$$\text{Azimuthal} \quad : ne\nabla_\theta V - \nabla_\theta P - J_\perp B + \frac{m_e \nu}{e} j_\theta = 0 \qquad (19)$$

$$\text{Parallel to B}: ne\nabla_{\parallel} V - \nabla_{\parallel} P + \frac{m_e \nu}{e} j_{\parallel} = 0 \quad . \qquad (20)$$

Because the electron mobility along magnetic field lines is much greater than the mobility across the field it is reasonable to assume that there are no steady state potential or density gradients parallel to the magnetic field. Thus Eq. (20) becomes,

$$j_{\parallel} = 0 \qquad (21)$$

that is, there is no net current flow along magnetic field lines. Similarly it can be assumed that no steady state potential or density

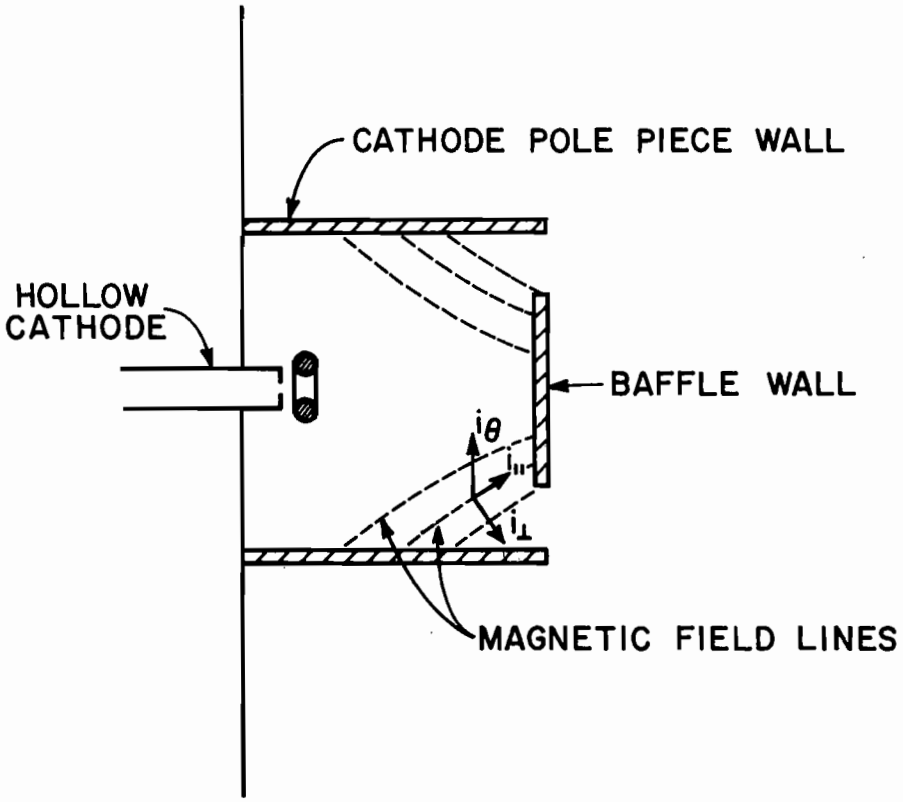

Fig. 5 Definition of Local Coordinate System

gradients exist* in the azimuthal direction due to symmetry. Thus Eq. (19) can be written as,

$$j_\theta = \frac{\omega}{\nu} j_\perp \tag{22}$$

where $\omega = eB/m_e$ is the electron cyclotron frequency. This equation says that no current can flow out of the aperture, $j_\perp$, unless there is also a current in the azimuthal direction.[17] Finally Eq. (18) can be solved for $j_\perp$ to obtain,

$$j_\perp = -\left[\frac{\nu e}{m_e(\nu^2 + \omega^2)}\right]\left(ne\nabla_\perp V - \nabla_\perp P\right) . \tag{23}$$

This equation can be written in terms of the classical diffusion coefficient defined by,[24]

$$D_c = \left[\frac{\nu}{\nu^2 + \omega^2}\right]\frac{kT}{m_e} . \tag{24}$$

to yield,

$$j_\perp = - D_c \left(\frac{e}{kT}\right)\left(ne\nabla_\perp V - \nabla_\perp P\right) . \tag{25}$$

For the magnetic field strengths and densities in the aperture region it was found that, $\omega/\nu >> 1$, (see Appendix B), therefore ν^2 may be neglected relative to ω^2 in the denominator of Eq. (24) to obtain,

$$D_c = \frac{kTm_e\nu}{e^2B^2} . \tag{26}$$

Diffusion coefficients calculated from Eq. (26) have often been found to be inadequate for use in typical ion thruster plasmas,[12,25] predicting coefficients sometimes orders of magnitude smaller than

---

* Plasma oscillations leading to potential gradients in the azimuthal direction have been proposed as a mechanism for anamolous diffusion. However, it is asserted here that no steady state potential gradients exist, while maintaining that anamoulous diffusion is still possible.

experimentally observed values. This failure of the classical theory is attributed to the enhancement of the diffusion mechanism by plasma turbulence.[26] A simple and well known semiemperical approach to turbulent electron diffusion was given by Bohm[27] as,

$$D_B = \frac{kT}{16eB} \quad . \tag{27}$$

Although this theory has been shown to work much better in the main discharge chamber of an ion thruster than the classical theory,[12,25] it is still only accurate to within a factor of 2 or 3.[27] Calculations presented in Appendix B indicate that Bohm diffusion also yields better results in the baffle aperture region than classical diffusion theory. Therefore in spite of the factor of 2 or 3 uncertainty, Bohm diffusion will be used in the remainder of the analysis because of its simplicity and relatively good agreement with experimental results. Using Eq. (27) in place of the classical diffusion coefficient in Eq. (25) yields,

$$j_\perp = - \frac{1}{16B} (ne\nabla_\perp V - \nabla_\perp P) \quad . \tag{28}$$

Now making the change of notation, $\nabla_\perp \rightarrow \frac{d}{dr}$ *, Eq. (28) can be written in the form,

$$j_\perp = - \frac{1}{16B} \left(ne \frac{dV}{dr} - \frac{dP}{dr}\right) \tag{29}$$

or,

$$-16 j_\perp B dr = ne dV - dP \quad . \tag{30}$$

Integrating over the diffusion depth[28] yields,

---

* This change of notation is appropriate when the net electron current flow out of the aperture is in the radial direction. If the current flows in the axial direction then $\nabla_\perp \rightarrow \frac{d}{dz}$ should be used.

$$-16\int j_{\perp} B dr = e\int ndV - \int dP \quad . \tag{31}$$

The current density, $j_{\perp}$, can be written as,

$$j_{\perp} = \frac{I}{A} \tag{32}$$

where, A, is the area through which the current* (I) flows in the aperture. Neglecting ionizations in the aperture region the current, I, must be constant to satisfy continuity. The area through which the current flows however is not constant due to the cylindrical geometry and magnetic field configuration, and therefore it must be left under the integral sign. Thus Eq. (31) can be written as,

$$-16\ I \quad \int \frac{B}{A}\, dr = e\int ndV - \int dP \tag{33}$$

or

$$I = -\frac{e\int ndV - \int dP}{16\int \frac{B}{A} dr} \quad . \tag{34}$$

This is the desired theoretical relationship between the current through the aperture and the geometry, magnetic field and plasma properties around the baffle aperture region.

Simplifications

Although Eq. (34) provides a theoretical relationship between the parameters of interest it is undesirable, in its present form, for the following reason. Evaluation of the integrals on the right-hand side

---

* The current through the aperture due to the motion of the electrons is given the symbol (I) in this analysis and is in accordance with the standard current convention. Thus the current denoted by this symbol is related to the electron current through the aperture described in Eq. (5) by, $I = -I_{e_a}$.

of this equation requires a detailed knowledge of the plasma properties through the aperture. This is not in keeping with the objectives of the investigation specified in Chapter II. Consequently some simplication of Eq. (34) is in order. The second integral in the numerator of Eq. (34) can be integrated directly to yield,

$$\int dP = \Delta P \tag{35}$$

where, ΔP, is simply the difference in electron pressure between the main and cathode discharge regions. Since the velocity distribution in the cathode region is approximately Maxwellian,* the pressure can be determined from,

$$P_c = n_c k T_c \tag{36}$$

where the subscript "c" refers to cathode region properties. The electron pressure on the main discharge side is the sum of the pressures due to the Maxwellian and primary electron populations, that is

$$P_m = n_m k T_m + P_p \tag{37}$$

where the subscript "m" refers to main discharge region properties and P_p is the pressure due to the primary electrons. This pressure can be found from the relation[29]

$$P_p = n_p m_e \bar{w} \bar{w} \tag{38}$$

where m_e is the electron mass and $\bar{w}$ is the average primary electron

---

* Some Langmuir probe trace measurements did indicate the presence of $\sim$10 eV primaries in the cathode region. Presumably these primaries are created by being accelerated from the cathode orifice across the electrostatic sheath which separates the plasma from the cathode, and into the cathode region. Inclusion of these primaries in the data analysis was found to have a negligible effect, and they will therefore be neglected.

speed. This speed can be determined from,

$$\tfrac{1}{2} m_e \bar{w}^2 = \varepsilon_p \tag{39}$$

where ε_p is the primary electron energy. Combining Eqs. (35), (36), (37), (38) and (39) yields,

$$\int dP = \Delta P = n_m k T_m + 2 n_p \varepsilon_p - n_c k T_c \quad . \tag{40}$$

Simplification of the term, $\int ndV$, in Eq. (34) is a little less straightforward. Figure 6 shows the density and potential variation through a typical baffle aperture.* These and other data not presented suggest that a reasonable approximation to the term, $\int ndV$, can be obtained from,

$$\int ndV \simeq \bar{n} \Delta V \tag{41}$$

where ΔV is the change in potential across the aperture and $\bar{n}$ is the average value of the density defined by,

$$\bar{n} = \frac{n_m + n_c}{2} \quad . \tag{42}$$

Combining Eqs. (34), (35) and (41), yields,

$$I \simeq - \frac{e \bar{n} \Delta V - \Delta P}{16 \int \frac{B}{A} dr} \tag{43}$$

where ΔP and $\bar{n}$ are determined from Eqs. (40) and (42) respectively. Equation (43) now is an approximate version of Eq. (34) and requires as inputs plasma data from only two points, the cathode and main discharge regions. The integral in the denominator of Eq. (43) was left intact because the strength and configuration of the magnetic field

---

* These measurements were actually made in the radial field thruster described in the next chapter. In this thruster the direction perpendicular to the magnetic field (horizontal axis) is the radial direction.

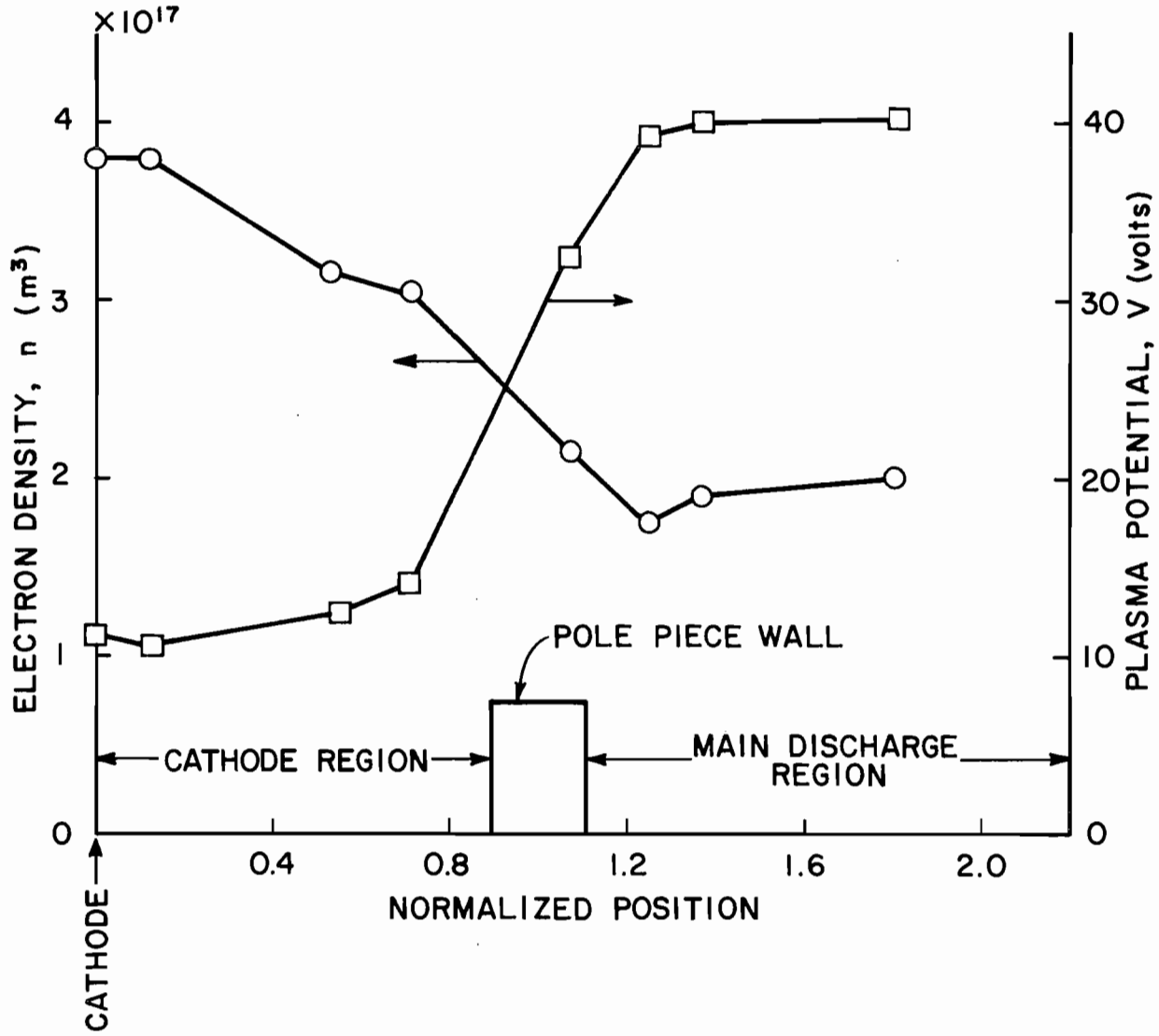

Fig. 6 Typical Plasma Density and Potential Variations Through the Baffle Aperture

as well as the aperture area are under the direct control of the designer, and thus the integral can easily be specified, a priori.

IV. APPARATUS

Although the aperture region was of prime consideration for this study it must be investigated as part of a complete thruster. Therefore, the two very different thruster configurations described below were tested.

Radial Field Thruster

Tests were conducted on the radial field thruster[30] shown schematically in Fig. 7. For this thruster and cathode pole piece geometry the electron current emitted by the cathode flows axially into the cathode discharge region. From there the current is driven radially out of the cathode region across the aperture region magnetic field. The electrons diffuse across the magnetic field lines in the baffle aperture until they reach a field line which carries them into the main discharge region. This field line is called the critical magnetic field line.

This thruster consisted of a 14 cm diameter source equipped with a set of dished accelerator system grids. The accelerator grid had a 54 percent open area fraction and was maintained at -500 volts, while the screen grid had a 67 percent open area fraction and was operated at +1000 volts. Eight radially oriented electromagnets were used to control the strength of the magnetic field in the main discharge region. The thruster was equipped with the magnetic baffle/pole piece assembly shown in detail in Fig. 8. This magnetic baffle assembly allowed the magnetic field strength in the aperture region to be varied over a wide range of values through the use of a 12 turn solenoid. The magnetic coupling rods shown were made of soft iron (as were the pole

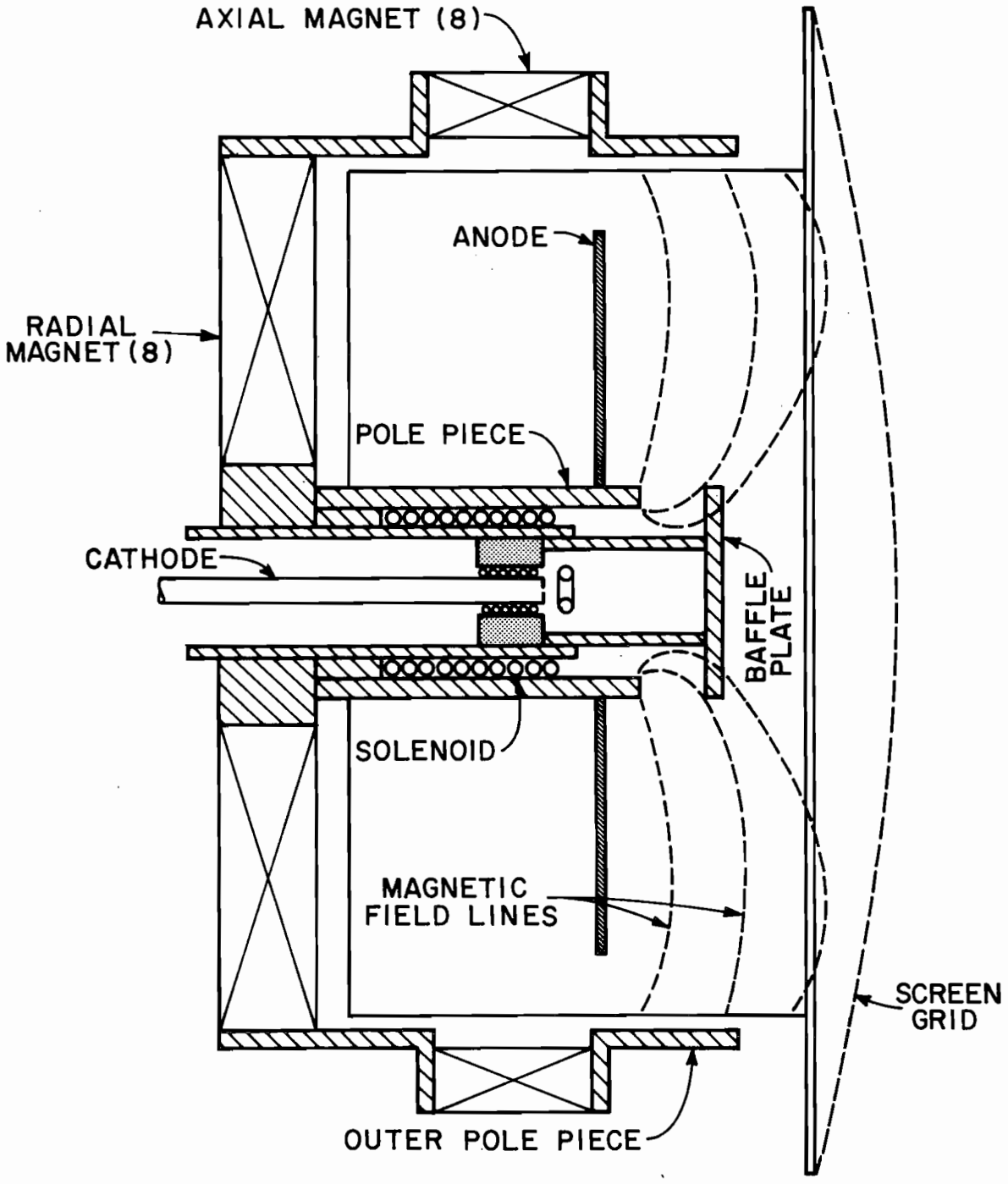

Fig. 7 Radial Field Thruster Equipped with Magnetic Baffle

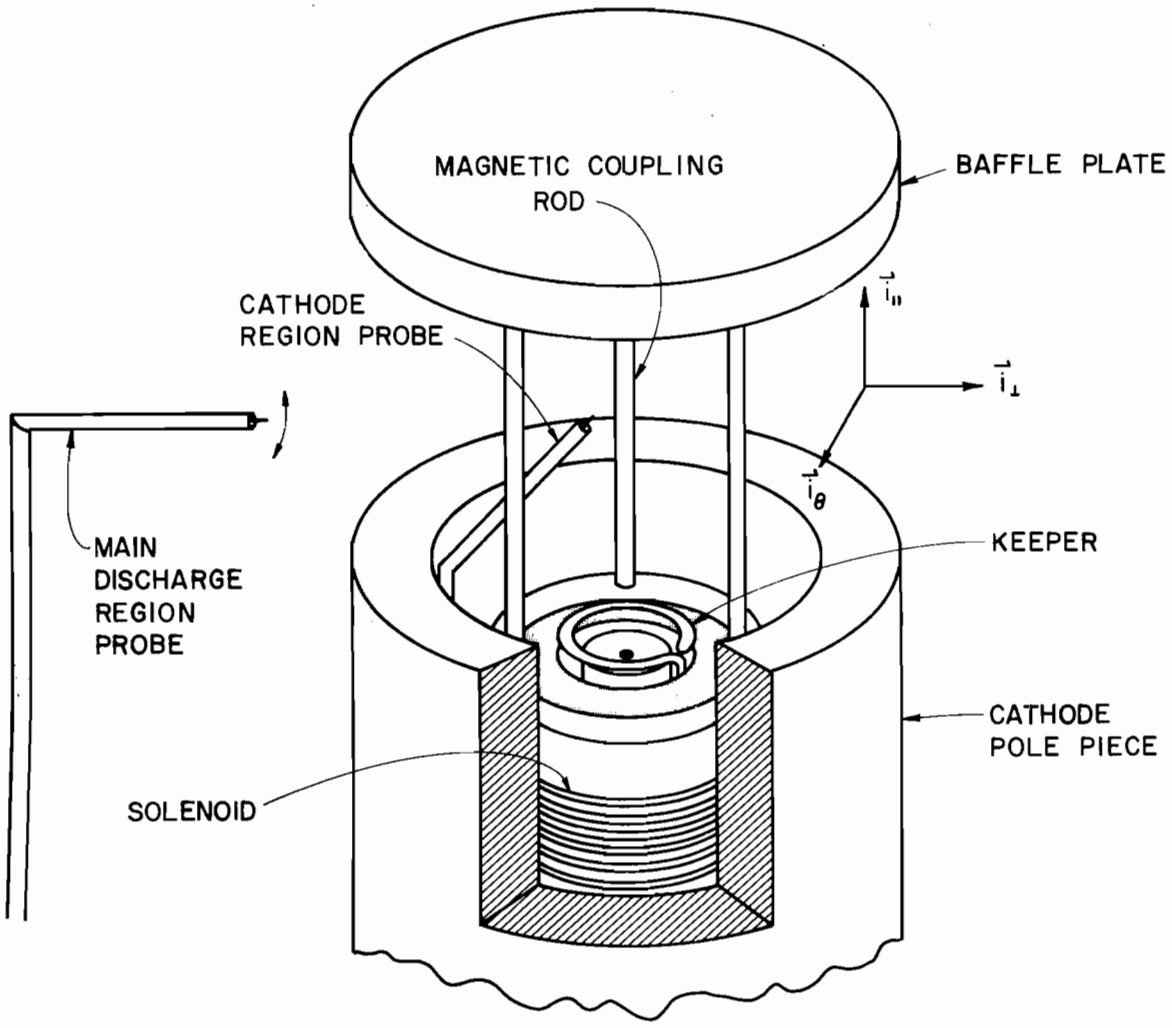

Fig. 8 Cathode Pole Piece/Baffle Assembly for Radial Field Thruster

piece and baffle plate) and were of suffient cross section to assure that the magnetic flux through the rods was well below the saturation point at the maximum solenoid current used. Since the cathode pole piece was part of the main thruster's magnetic circuit, changing the current through the radial magnets changed the magnetic field strength in the aperture as well as in the main discharge region. However, changing the field strength in the aperture by using the baffle magnetic solenoid did not significantly change the magnetic field in the main discharge region. This allowed data for testing the model, to be collected over a wide range of magnetic field variations.

Two cylindrical Langmuir probes were used to measure the plasma properties on each side of the aperture. The cathode region probe was a 0.076 cm diameter wire, 0.076 cm long supported from a quartz tube insulator. It was positioned at a radial distance approximately equal to the keeper radius at the axial midpoint of the aperture gap. The main discharge region probe was a 0.076 cm diameter wire, 0.123 cm long again supported from a quartz insulator. The positioning of both probes can be seen in Fig. 8. The main discharge region probe could also be swept radially through the aperture to facilitate the measurement of plasma properties as a function of radial position.

Multipole Thruster

Additional tests were conducted on the multipole thruster[31] shown schematically in Fig. 9. This was a 15 cm diameter source equipped with the same grid set used on the radial field thruster. Thirty-two electromagnets wired in series were used to control the strength of the magnetic field protecting the anodes. This thruster was outfitted

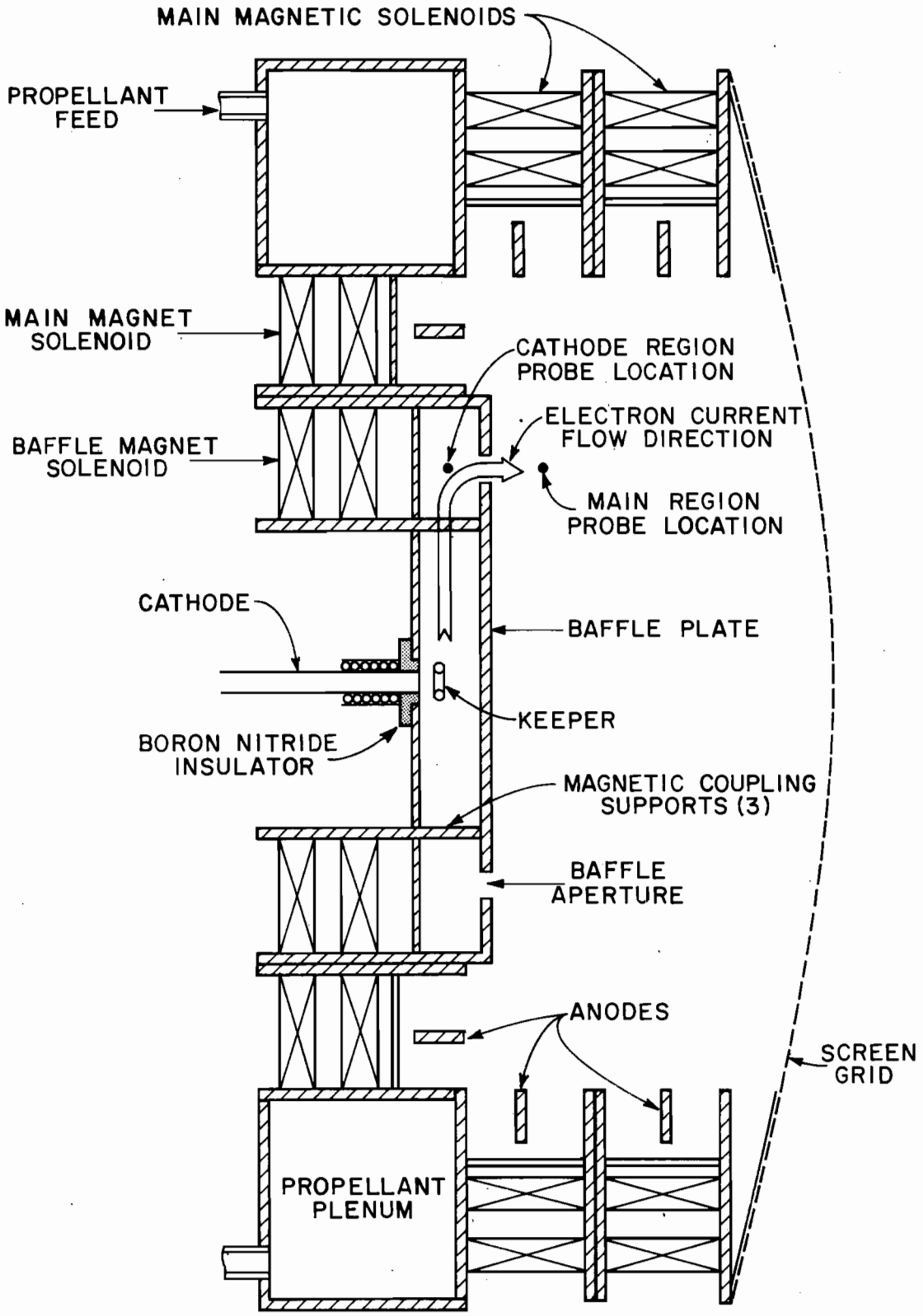

Fig. 9 Multipole Thruster with Large Cathode Region/Magnetic Baffle Assembly

with an abnormally large cathode region/magnetic baffle assembly* which provided a radically different geometry from that of the radial field thruster on which to test the model. The direction of electron current flow through the aperture is also indicated in Fig. 9.

Again two probes similar in construction to the probes used on the radial thruster, were used to measure the plasma properties on each side of the aperture. Because the magnetic field created by the baffle electromagnets was concentrated in the aperture region only, the cathode region probe was positioned out at the radius of the aperture and not over the keeper as it was for the radial field thruster. The positions of both probes can be seen in Fig. 9. The thruster was operated with the cathode region/magnetic baffle assembly extended $\sim$1 cm into the main discharge region as suggested by Longhurst[31] to assure that electrons leaving the baffle aperture were not immediately captured by the magnetic fringe field of the inner most anode ring. Finally the cathode was electrically isolated from the thruster body so that the net electron current emitted by the cathode could be measured directly during operation.**

Operation of both thrusters was conducted in the 1.2 m diameter, 4.6 m long vacuum facility at the Engineering Research Center of

---

* Another cathode region baffle assembly utilizing two hollow cathodes was also tested in this multipole thruster. The results of this test are given in Appendix C.

** The details of this measurement are described in Appendix D.

Colorado State University. The facility pressure was maintained below 1×10^{-5} torr for all tests.

V. PROCEDURE

In order to test the baffle aperture model developed in Chapter III experimentally, Eq. (43) was rewritten in the form,

$$\bar{e}\bar{n}\Delta V - \Delta P = - 16I\int\frac{B}{A}\,dr \quad . \tag{44}$$

This equation is now in a form which states that the plasma properties on the left-hand side of this equation are a function of the parameters on the right-hand side. That is, the plasma properties in Eq. (44) should change in accordance with changes in either the current through the aperture (I), the aperture region magnetic field strength (B) or the area through which the current flows (A). In addition these quantities, the current, magnetic field strength and aperture area can easily be controlled by the experimenter.

Consequently the following experimental procedure was implemented for the collection of data on the radial field thruster. Before each test run the aperture area was set by adjusting the distance between the downstream edge of the cathode pole piece and the baffle plate. Three different aperture areas were tested. During thruster operation the current through the aperture was indirectly varied by changing the current through the discharge power supply. In addition the magnetic field strengths in the aperture and main discharge regions were varied by changing the currents through the radial and baffle electromagnets. The magnetic field strength in the main discharge region was varied from $\sim$ 7 to 45 x 10^{-4} tesla, while the field in the aperture region was varied over the range of 9 to 110 x 10^{-4} tesla. These changes resulted in an order of magnitude variation in the beam current, from $\sim$ 40 to 485 mA. At each discharge current, magnetic field and aperture

area setting tested the following data was collected. Langmuir probe* traces, from which the plasma properties of interest can be determined, were taken in both the cathode and main discharge regions and the discharge current, discharge voltage, beam current, keeper voltage and electromagnet currents were recorded. In addition to the above mentioned variations the cathode and main neutral flow rates were varied over the ranges 80-200 and 400-600 mA eq. respectively. The neutral flow rate measurements were made approximately every 30 minutes by timing the drop a liquid mercury column in a precision bore glass tube. After shutdown of the thruster and its subsequent removal from the vacuum system the magnetic field strength through the aperture was measured with a two-axis gauss meter. The magnetic field strength was measured for each setting of radial and baffle electromagnet current at which Langmuir probe traces were recorded.

The procedure used on the radial field thruster was also followed for the collection of data on the multipole thruster with the exception that the net cathode emission current was also recorded at each operating condition tested. A summary of the parameters varied in the tests on both thrusters is provided in Table I.

---

* Both Langmuir probes were cleaned by ion bombardment[32] before any traces were taken. Probe traces were analyzed using a program developed by Beattie.[33]

Table I

Test Conditions

Test No.	Thruster	Aperture Area (10^{-4} m^2)	Flow Rate Range (mA eq.)		Aperture Current [A]	Aperture Magnetic Field Strength (10^{-4} tesla)
			Cath.	Main		
1	Radial	5.7	153-200	650	3.0-4.5	9-111
2	Radial	6.9	102-158	475-510	2.3-3.4	15-107
3	Radial	9.1	80-100	406-500	2.2-3.5	13-100
4	Multipole	11.0	200-250	400-450	1.5-3.2	10- 33

VI. EXPERIMENTAL RESULTS AND DISCUSSION

Baffle Aperture Current

Measurement of the net cathode emission current during the operation of the multipole thruster as well as the discharge current and beam current allowed the two methods developed in Chapter II for determining the current through the aperture to be compared. Combining Eqs. (5) and (11) yields,

$$I_E = I_D - I_{i_b}\left[\frac{A_w + A_s}{A_s}\right]. \tag{45}$$

That is, the net cathode emission current should approximately equal the discharge current minus the ion flux to the beam and to cathode potential surfaces. A comparison of the theory with the experimental results is given in Fig. 10. The best fit was obtained when the effective screen grid open area (A_s) was taken to be the entire area covered by the grid. This assumes that every ion that encounters the accelerator system gets extracted into the beam and none recombine on the screen grid webbing. Clearly the data of Fig. 10 suggest that the current through the baffle aperture can be determined using Eq. (45) and measured anode and beam currents.

Comparison of Model with Experiment

To test the validity of Eq. (43) experimentally it was found more convenient for the presentation of the results to rewrite it in the form,

$$\int \frac{B}{A}\, dr = -\frac{1}{16I}\left[e\bar{n}\Delta V - \Delta P\right] . \tag{46}$$

Thus the value of the integral, $\int \frac{B}{A}\, dr$, computed from Eq. (46) using measured plasma data can be compared to the value determined from measuring the magnetic field and area variation through the aperture directly. A description of the procedure used to measure the value of this integral directly is given in Appendix E.

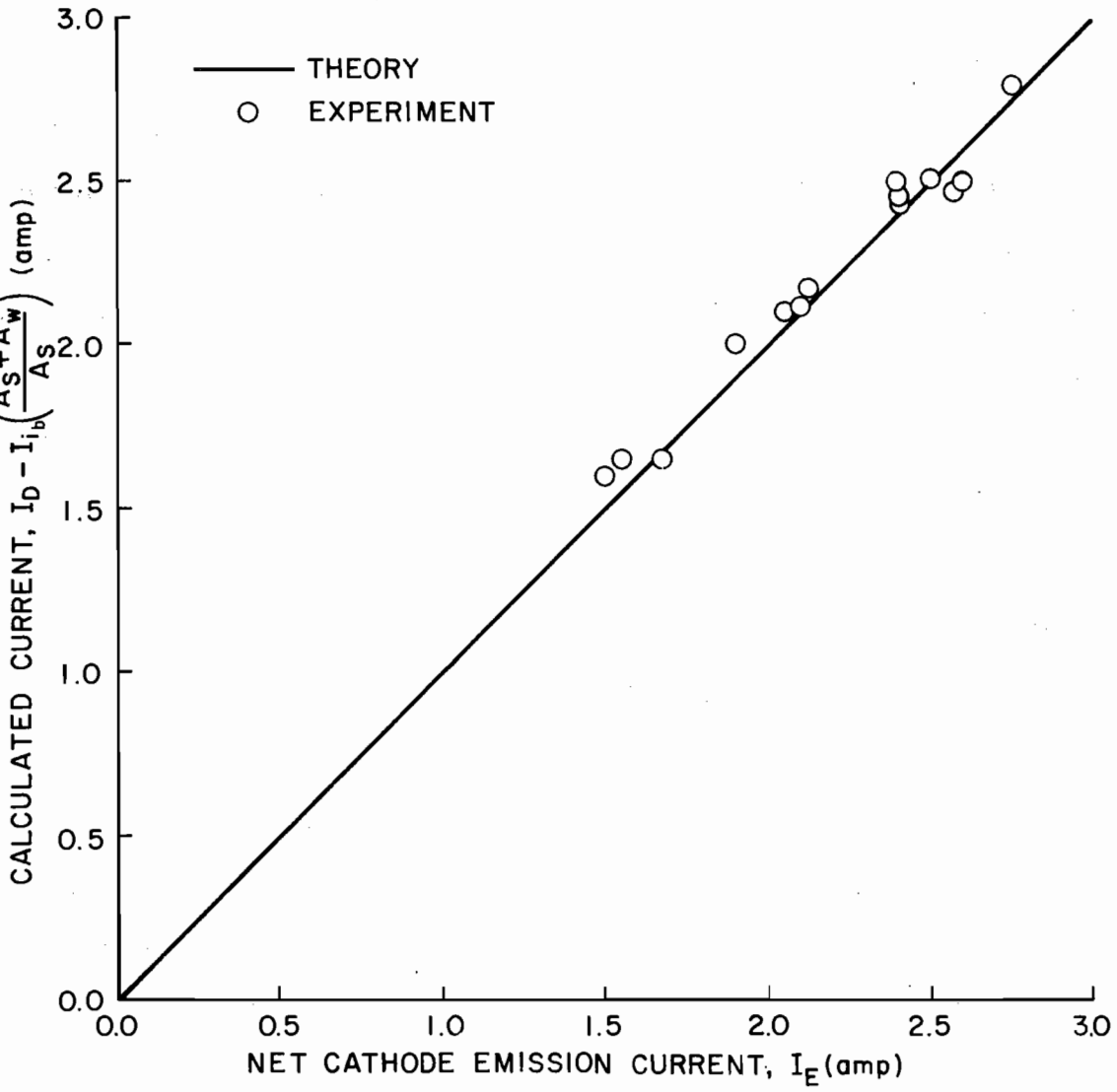

Fig. 10 Comparison of Methods for Determining the Baffle Aperture Current

The results of the comparison of the integrals calculated by the theory (Eq. (46)) to the directly measured values for the radial field thruster is given in Fig. 11, where the solid line represents a linear least squares curve fit forced to go through the origin. This line has a correlation coefficient of 0.83 and a slope of $\frac{1}{2}$. The different symbols represent the different test configurations listed in Table I. The theory is seen to yield remarkably consistant results even over extreme changes in thruster operating conditions. The scatter observed in the data is believed to be due at least in part to experimental error. The single largest source of error being the analysis of Langmuir probe data. The amount of scatter is believed to be good when compared to other studies of this nature. Ideally, however, the curve fit should have a slope of unity if the model is exactly correct. As it stands, the model predicts values of the integral that are a factor of two low. It is noted however that this is within the accuracy of the Bohm diffusion coefficient. Consequently a straightforward method to obtain good agreement between the model and experiment would be to change the constant $\frac{1}{16}$ in the Bohm diffusion formula. The value $\frac{1}{16}$ has no theoretical justification but is an empirical number agreeing with most experiments to within a factor of two or three.[34] An experimental fit of this constant by Spitzer[35] yielded a value of 0.21 and Yoshikawa and Rose[26] give the constant in the range 0.031 to 0.063 depending on the magnitude of the density fluctuation. However, both of these studies as well as Bohm's original work were conducted at magnetic field strengths and plasma densities much greater than those normally found in an ion thruster. In the few diffusion studies actually conducted in operating ion thrusters[12,25,36] which employed Bohm diffusion only Robinson[36] obtained

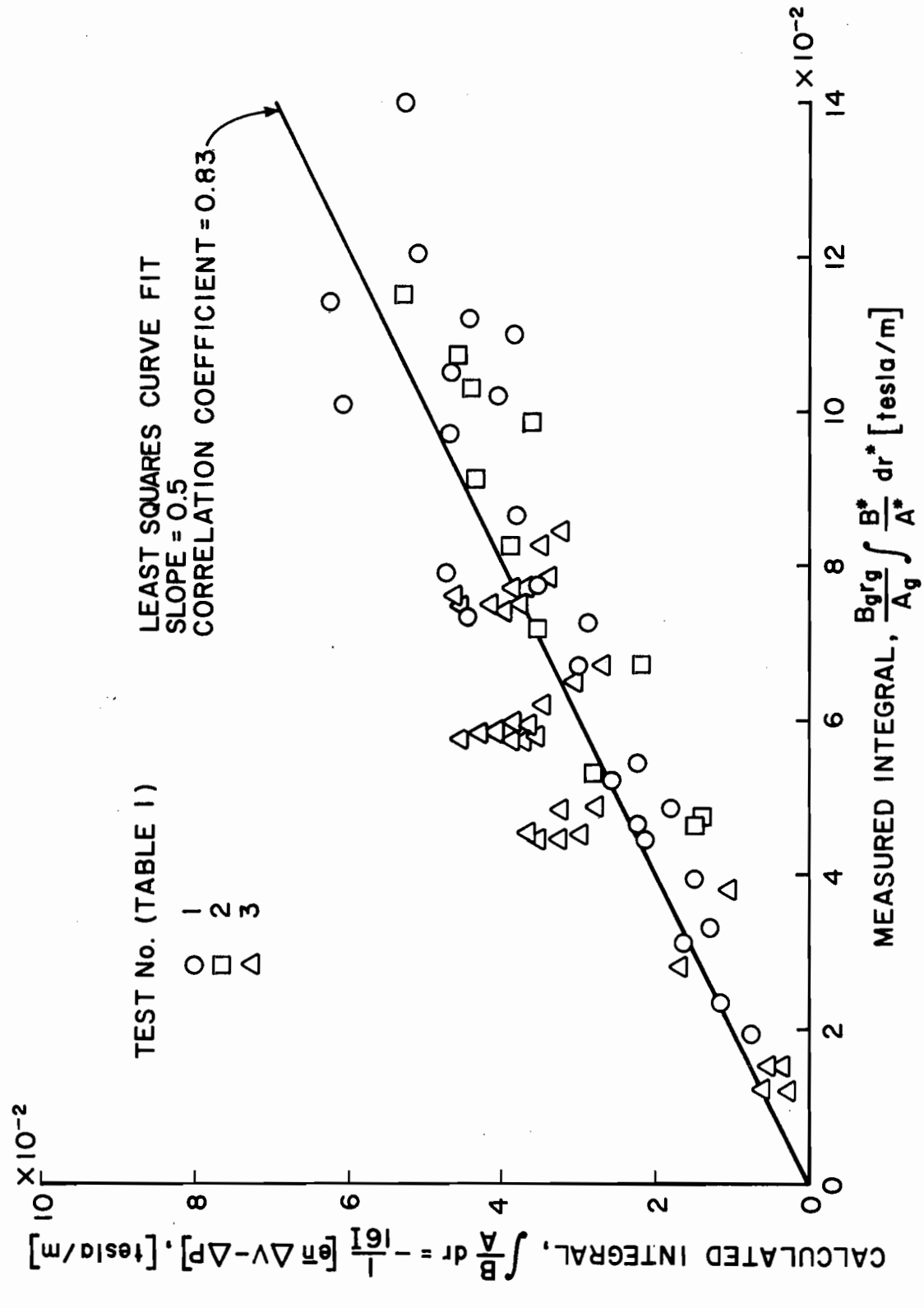

Fig. 11 Comparison of Calculated Integrals with the Measured Values for the Radial Field Thruster

results which were good to better than a factor of two or three. Consequently it is not too surprising that the coefficient is off by a factor of two. A more important result is the minimum of scatter observed over substantial changes in operating parameters. Good agreement between the model and experiment would be obtained in this case for an empirical constant of $\frac{1}{8}$ rather than $\frac{1}{16}$.

It was of interest to test the model on a radically different cathode region and thruster geometry from that of the radial field thruster. The multipole thruster of Fig. 9 meets this requirement. The major differences between this thruster geometry and that of the radial field thruster are the following. First, the current flows essentially in the axial direction through the aperture rather than radially. Second, the large size of the cathode region means that the mean diameter of the aperture is considerably larger in this case as is the distance between the cathode itself and the aperture. This makes the coupling between the cathode and the anode more difficult. Finally the main discharge region is essentially magnetic field free making less obvious the location of the critical magnetic field line from which electrons find access to the main discharge. Due to the axial current flow direction through the aperture for this thruster, Eq. (43) must be written in the form,

$$\int \frac{B}{A} dz = - \frac{1}{16I} \left(e\bar{n} \Delta v - \Delta P \right) \tag{47}$$

where z is in the axial direction. The measurement of $\int \frac{B}{A} dz$, for this geometry is also discussed in Appendix E. A comparison of results obtained from the calculations of Eq. (47) and the measured integrals is given in Fig. 12. For this case it is seen that the theory predicts values that are scattered about the line of perfect correlation with no

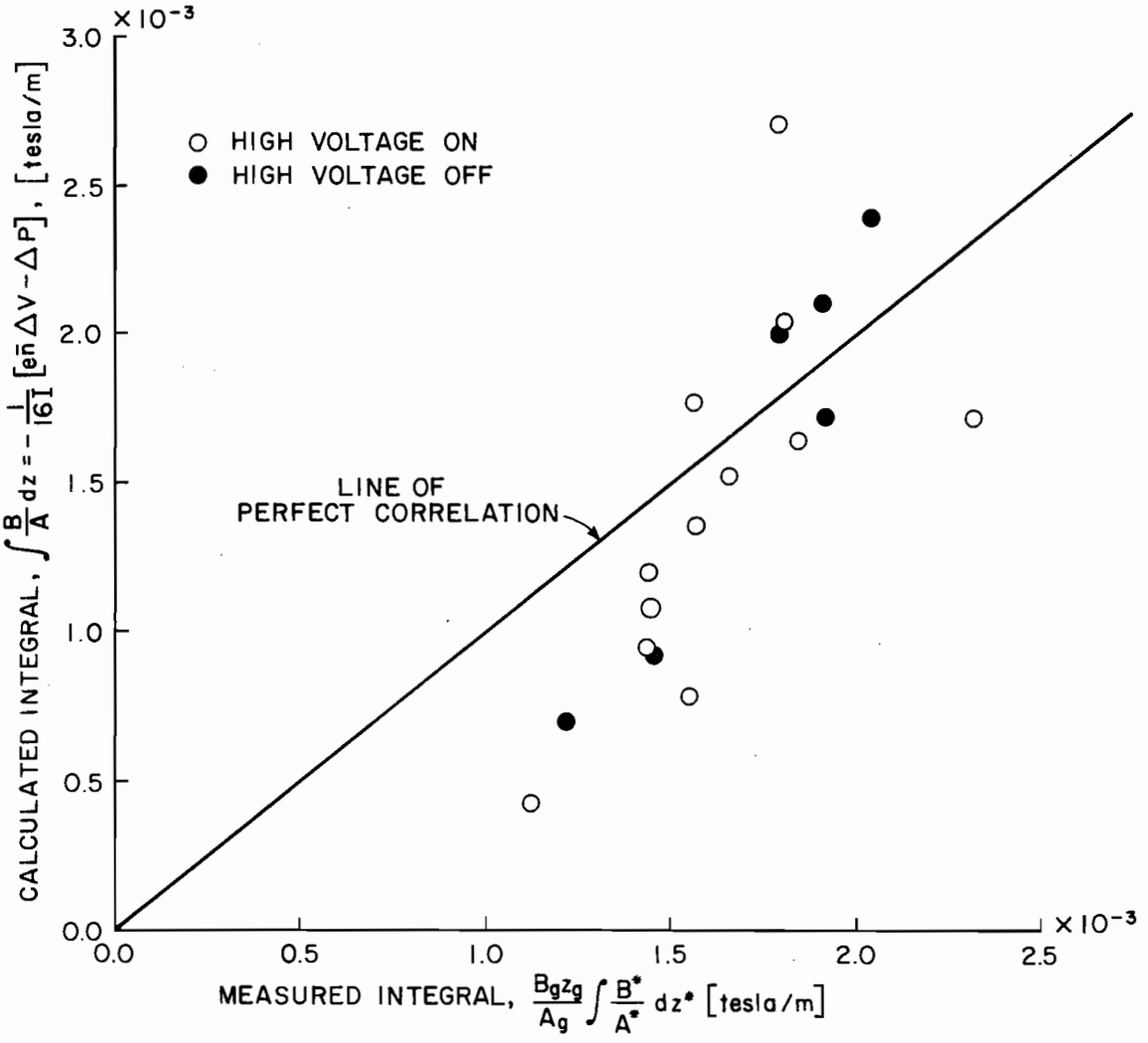

Fig. 12 Comparison of Calculated Integrals with the Measured Values for the Multipole Thruster

change of the empircal constant $\frac{1}{16}$ required. In addition the solid symbols in Fig. 12 indicate that the theory is independent of whether or not the high voltage is on as would be expected. It is not clear, however, why the model should agree correctly for this thruster geometry and be off by a factor of two for the radial field thruster geometry since one would expect the diffusion processes to be similar in both cases. It is possible however that a change such as that in the cathode pole piece geometry could change the nature of the turbulence which affects this empirical constant. It should also be pointed out that a considerably smaller range of values for the integral, $\int\frac{B}{A}\,dz$, was tested on the multipole thruster. This was primarily a result of the poor coupling between the cathode and the anode which prevented operation at higher aperture region magnetic field strengths. In any case this simple model has been shown to be correct to within a factor of 2 for extremely different cathode region geometries. In addition for each particular thruster geometry the theory is consistant over very substantial changes in operating conditions.

Inspection of Eq. (43) reveals that the electron current is driven through the aperture under the influence of two forces; the force due to the potential difference, $e\bar{n}\Delta V$, and the force due to the pressure difference, ΔP. It was of interest to calculate the relative magnitudes of these forces to determine which has the dominate effect. Table II lists the values of these terms for several cases covering a wide range of operating conditions. In addition the terms, $n_c kT_c$, $n_m kT_m$ and $2n_p\varepsilon_p$ which comprise ΔP according to Eq. (40) are also tabulated.

Table II

Comparison of Driving Forces
(Percent of Total)

Thruster Geometry	$\bar{e}n\Delta v$ (%)	ΔP (%)	$n_m kT$ (%)	$2n_p \epsilon_p$ (%)	$n_c kT_c$ (%)
Radial	90	10	- 3	-2	15
Radial	90	10	- 1	-0.4	12
Radial	94	6	- 8	-6	20
Radial	98	2	- 7	-0.3	8
Radial	106	-6	- 8	-6	7
Radial	103	-3	-16	-1	15
Multipole	99	1	-22	-14	37
Multipole	74	26	- 5	-4	34

Clearly the force due to the potential difference has the dominant effect. In fact in some cases the pressure force is seen to act in the direction opposite to the flow of electrons. Further, the contribution to the pressure from the primary electrons is seen to be generally small.

Design Usefulness

The design usefulness of the model is limited due to the factor of 2 or 3 uncertainty in the empirical constant in the Bohm diffusion model and the failure of the experimental results to establish firmly a new value for this constant of proportionality applicable to any baffle aperture geometry. Further, there is presently no model from which the cathode region plasma density can be calculated, and an a priori specification of this quantity can only be done approximately. The theory is still useful, however, in that the value of the required proportionality constant appears to be the same for a given thruster geometry over a wide range of operating conditions. Even considering the uncertainty the model could be used to provide a starting point for the cut and try design procedure. A brief description of how to apply the model to aid in the design of the baffle aperture region is provided below.

In general it would be desirable to be able to specify what open area and magnetic field strength are required for the aperture region to effect thruster operation at a given condition. This translates into the determination of the integral, $\int \frac{B}{A}\, dr$. It is seen that in order to calculate this integral from Eq. (46) (rewritten here for convenience),

$$\int \frac{B}{A}\, dr = - \frac{1}{16I} \left[e\bar{n} \Delta V - \Delta P \right] \tag{48}$$

the user must determine, a priori, the value of each of the quantities on the right-hand side of this equation. In general the designer of a thruster will know from other considerations the values of the beam current, discharge current and primary electron energy at which the thruster will operate. In addition the main discharge chamber geometry will be defined. Once the beam current has been specified the main discharge region density, n_m, can be found from the Bohm condition for a stable sheath which is expressed through the equation

$$I_{i_b} = A_s\, n_m e \sqrt{kT_m/m_i} \quad . \tag{49}$$

The use of Eq. (49) requires the user to supply a reasonable approximation for the main discharge region electron temperature, T_m, which can be taken to be $\sim$5 eV. As stated previously the plasma density in the cathode region is the most difficult parameter to specify and therefore will be a likely source of error. However, typical cathode region densities in this study were found to be of the order of 10^{18} m^{-3}. The electron temperature of the cathode region plasma can be taken to be approximately T_e = 23000°K (2eV). The density of the primary electrons in the main discharge region is also difficult to specify. Fortunately the pressure due to the primaries is small, as was shown earlier, and perhaps it can be neglected for these

calculations. Therefore the pressure difference, ΔP, can now be calculated in accordance with Eq. (40). In addition, the current through the aperture can be calculated from Eq. (11). Finally, the potential difference across the aperture can be approximated as the difference between the discharge voltage, V_D, and the keeper voltage,* V_k, as,

$$\Delta V = V_D - V_k \quad . \tag{50}$$

This difference should also be equal to the energy gained by the primary electrons after being accelerated through the aperture. Figure 13 shows the energy gained by the primaries, which was calculated as $\varepsilon_p - T_c$ in units of electron volts, plotted against the difference between the discharge and keeper voltages for the radial field thruster. Clearly this approximation is appropriate. Thus all the quantities on the right-hand side of Eq. (48) can be determined to one degree or another. The value of the integral $\int \frac{B}{A}\, dr$ can then be calculated and subsequently the baffle aperture region can be constructed to achieve this value.

Finally it is mentioned in passing that although the model is only certain to within a factor of 2 this is perhaps better than the certainty

---

* This was not true for the multipole thruster's cathode region used in this study because the large distance between the cathode and baffle aperture was accompanied by an increase in plasma potential over this distance. However this should be a reasonable approximation for more conventionally sized cathode regions where the distance from the cathode to the aperture region is comparable to the distance across the aperture region magnetic field.

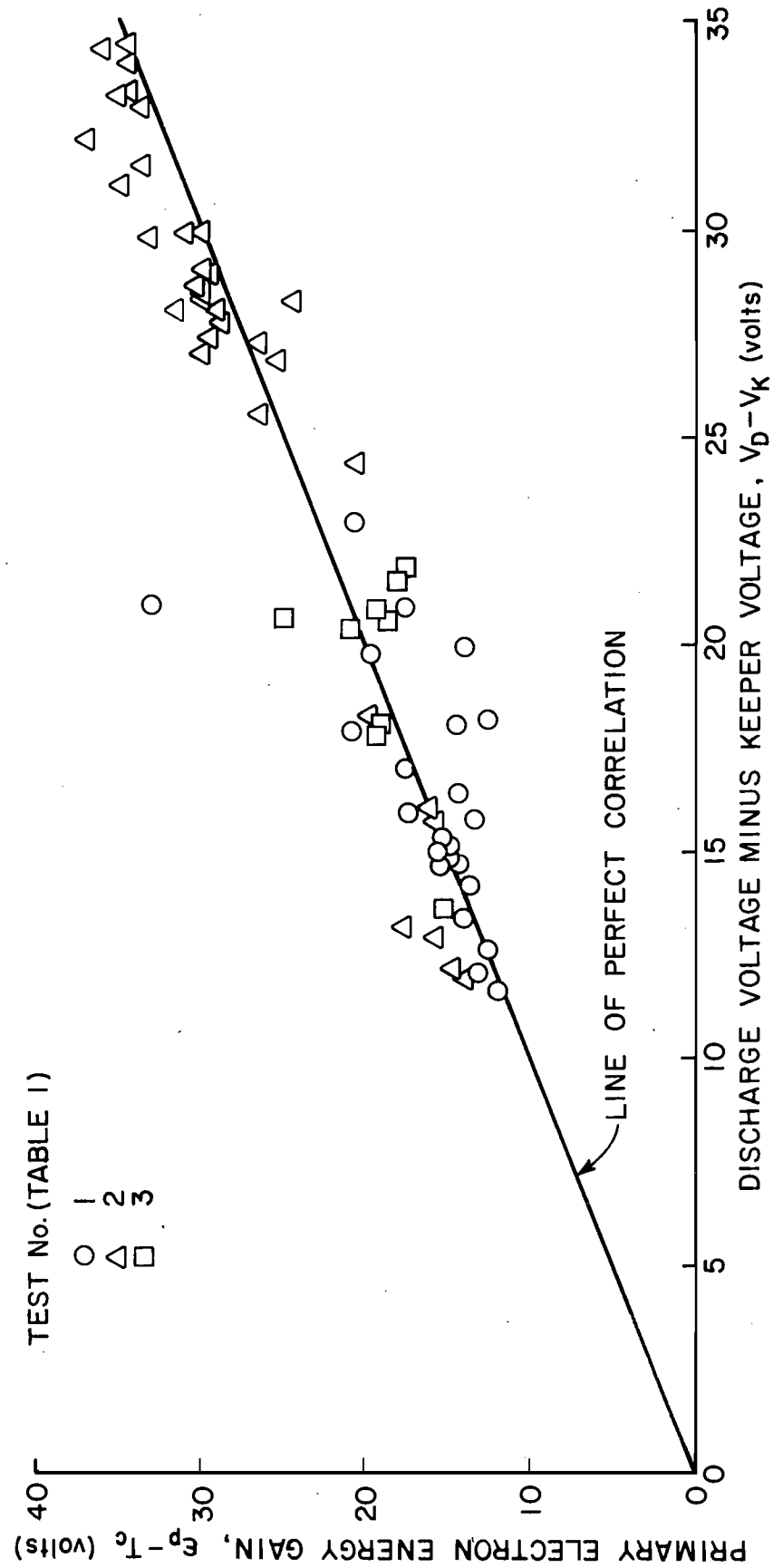

Fig. 13 Correlation of the Energy Gained by the Primary Electrons Through the Aperture with the Difference Between the Discharge and Keeper Voltages for the Radial Field Thruster

to which the plasma parameters required as inputs to the model can be specified. Also, it should be pointed out that the theory says nothing about where in the thruster's main discharge chamber the primary electrons should be injected, or where in the cathode discharge region the cathode should be located, or even what fraction of the total propellant flow rate should go through the cathode, all of which can influence thruster performance.

CONCLUSIONS

The following conclusions are drawn based on the study of the baffle aperture region.

1) The Bohm diffusion theory predicts values of the diffusion coefficient for the baffle aperture region which agree better with the experimentally determined values than does the classical theory.

2) The classical (collisional) theory typically predicts values of the diffusion coefficient which are at least an order of magnitude to small.

3) The baffle aperture current can be measured directly by measuring the net cathode emission current.

4) The magnitude of the current through the baffle aperture can be calculated as the difference between the discharge current and the ion current which goes to cathode potential surfaces and into the ion beam. These calculated values agree well with the measured values.

5) The simplified theoretical model of the baffle aperture region agrees correctly with the experimental results for the multipole thruster/cathode discharge region geometry. On the radial field thruster the model differs consistantly from the experimental results by a constant factor of two.

6) The potential difference across the aperture is the dominant force driving the electron current across the baffle aperture magnetic field lines into the main discharge region.

Future work should focus on the development of a model which can be used to determine the plasma properties of the cathode discharge region. In addition an in depth study of the relationships between the electron diffusion mechanism, the plasma turbulence characteristics

(frequency, magnitude) and the cathode discharge region geometry might be necessary to determine why there appeared to be a factor of two difference between the results obtained on the radial and multipole thrusters.

REFERENCES

1. Bechtel, R. T., Csiky, G. A. and Byers, D. C., "Performance of a 15-centimeter Diameter, Hollow-Cathode Kaufman Thruster," AIAA Paper No. 68-88, New York, New York, Jan. 22-24, 1968.

2. Bechtel, R. T., "Performance and Control of a 30-cm. dia. Low-Impulse, Kaufman Thruster," AIAA Paper No. 69-238, Williamsburg, VA, March 3-5, 1969.

3. King, H. J., Poeschel, R. L. and Ward, J. W., "A 30-cm Low-Specific Impulse, Hollow-Cathode Mercury Thruster," AIAA Paper No. 69-300, Williamsburg, VA, March 3-5, 1969.

4. Poeschel, R. L., Ward, J. W. and Knauer, W., "Study and Optimization of 15-cm Kaufman Thruster Discharges," AIAA Paper No. 69-257, Williamsburg, VA, March 3-5, 1969.

5. Palumbo, G., et. al., "Effect of Geometry and Field Inside the Pole Piece in an Electron Bombardment Thruster," AIAA Paper No. 70-1082, 1970.

6. Poeschel, R. L. and Vahrenkamp, R., "The Radial Magnetic Field Geometry as an Approach to Total Ion Utilization in Kaufman Thrusters," AIAA Paper No. 72-481, April 17-19, 1972.

7. Masek, T. D., "Plasma Properties and Performance of Mercury Ion Thrusters," AIAA Paper No. 69-256, 1969.

8. Medicus, G., "Diffusion and Elastic Collision Losses of the 'Fast Electrons' in Plasmas," Journal of Applied Physics, Vol. 29, No. 6, p. 903, June 1958.

9. Cohen, A. J., "Onset of Anomalous Diffusion in Electron-Bombardment Ion Thruster," NASA Paper TN D-3731, Nov., 1966.

10. Poeschel, R. L. and Vahrenkamp, R., "The Radial Magnetic Field Geometry as an Approach to Total Ion Utilization in Kaufman Thrusters," AIAA Paper No. 72-481, Bethesda, MD, April 17-19, 1972.

11. Beattie, J. R., "Cusped Magnetic Field Mercury Ion Thruster," Ph.D Thesis, July 1976, Department of Mechanical Engineering, Colorado State University, Fort Collins, Co.

12. Isaacson, G. C., "Multipole Gas Thruster Design," Ph.D Thesis, June 1977, Department of Physics, Colorado State University, Fort Collins, Co.

13. Longhurst, G. R., "Prediction of Plasma Properties in Mercury Ion Thrusters," Ph.D. Thesis, December 1978, Dept. of Mechanical Engineering, Colorado State University, Fort Collins, Co.

14. Weigand, A. J. and Nakanishi, S., "A Survey of Kaufman Thruster Cathodes," NASA TM X-67918, 1971.

15. Bohm, D., "Minimum Ionic Kinetic Energy for a Stable Sheath," in, Characteristics of Electrical Discharges in Magnetic Fields, A. Guthrie and R. K. Wakerling, eds., McGraw-Hill, Inc., New York, 1949.

16. Wilbur, P. J., "An Experimental Investigation of a Hollow Cathode Discharge," NASA CR-120847, December, 1971.

17. Wells, A. A., "Current Flow Across a Plasma 'Double Layer' in a Hollow Cathode Ion Thruster," AIAA Paper No. 72-418, April 17-19, 1972.

18. Poeschel, R. L. and Kanauer, W., "A Variable Magnetic Baffle for Hollow Cathode Thrusters," AIAA Paper No. 70-175, Jan. 19-21, 1970.

19. Poeschel, R. L., "The Variable Magnetic Baffle as a Control Device for Kaufman Thrusters," AIAA Paper No. 72-422, April 17-19, 1972.

20. Longhurst, G. R., "Magnetic Baffle for 15 cm. Multipole Mercury Thruster," in Appendix A of "15 cm. Mercury Ion Thruster Research-1976," ed. P. J. Wilbur, NASA CR-135116, December, 1976.

21. Beattie, J. R., "Single Cusp Magnetic Field Thruster," in "Hollow Cathode Restartable 15 cm. Diameter Ion Thruster," ed P. J. Wilbur, NASA CR-134532, December 1976.

22. Chen, F. F., Introduction to Plasma Physics, Plenum Press, New York, 1974, Chp. 3, p. 57.

23. Uman, M. A., Introduction to Plasma Physics, McGraw-Hill, Inc., 1964, p. 168.

24. Jahn, R. G., Physics of Electric Propulsion, McGraw-Hill, Inc., New York, 1968, Chp. 5.

25. Longhurst, G. R., "The Diffusion of Electrons in Ion Thrusters," in, "Mercury Ion Thruster Research-1977," Paul Wilbur, ed., NASA CR-135317, December, 1977.

26. Yoshkawa, S. and Rose, D. J., "Anomalous Diffusion of a Plasma Across a Magnetic Field," Physics of Fluids, Vol. 5, No. 3, March, 1962, p. 334-341.

27. Bohm, D., "The Use of Probes for Plasma Exploration in Strong Magnetic Fields," in Characteristics of Electrical Discharges in Magnetic Fields, A. Guthrie and R. K. Wakerling, eds., McGraw-Hill, Inc., New York, 1949.

28. Kaufman, H. R. and Robinson, R. S., "Plasma Processes in Inert Gas Thrusters," AIAA Paper No. 79-2055, Oct. 30-Nov. 1, 1979, Princeton, N.J.

29. Chen, F. F., loc. cit., Chp. 7, p. 212.

30. Longhurst, G. R., "Screen Anode Thruster," in "Mercury Ion Thruster Research-1977" P. J. Wilbur, ed., NASA CR-135317, December, 1977.

31. Longhurst, G. R. and Wilbur, P. J., "Multipole Mercury Ion Thruster," AIAA Paper No. 78-682, April 25-27, 1978.

32. Wehner, G. and Medicus, L., "Reliability of Probe Measurements in Hot Cathode Gas Diodes," J. Applies Physics, Sept. 1952.

33. Beattie, J. R., "Numerical Procedure for Analyzing Langmuir Probe Data," AIAA Journal, V. 13, No. 7. July 1975, pp. 950-952.

34. Chen, F. F., loc. cit., Chp 5, p. 169.

35. Spitzer, L., "Particle Diffusion Across a Magnetic Field," Physics of Fully Ionized Gases, Interscience Publishers, Inc., New York, 1956.

36. Robinson, R. S., "Physical Processes in Ion Beam Sputtering," Ph.D. Thesis, March 1979, Department of Physics, Colorado State University, Fort Collins, Co.

37. Wilbur, P. J., Monthly letter on NASA Grant NGR-06-002-112, June 5, 1980.

38. Holt, E. H. and Haskell, R. E., Plasma Dynamics, The MacMillan Company, New York, 1965, Chp. 9.

39. Wilbur, P. J., "Neutral Balance Model for the Cathode Discharge Region," in "Experimental Investigation of a Throttlable 15 cm. Hollow Cathode Ion Thruster," NASA Cr-12038, December, 1972.

APPENDIX A

MAGNITUDE OF NEGLECTED ION CURRENTS

In the derivation of Eq. (5) the ion current through the baffle aperture as well as the ion current to the cathode region walls were neglected. To show that this is appropriate the magnitudes of these currents will be calculated and compared to the electron current through the aperture for the worst cases observed.

The flux of ions that reach the cathode region walls is given by the formula,

$$\Gamma_{i_\omega} = A_c n_c \sqrt{\frac{kT_c}{m_e}} \qquad \text{(A-1)}$$

assuming they reach the sheath edge with the Bohm velocity.[15] Assuming singly charged ions, the ion correct to the walls then can be found from,

$$I_{i_\omega} = n_c e A_c \sqrt{\frac{kT_c}{m_c}} \quad . \qquad \text{(A-2)}$$

Equation (A-2) can now be used to calculate the ion current to the cathode region walls. The area available for ion recombination in the cathode region was about

$$A_c = 2.5 \times 10^{-4} \text{ m} \quad .$$

For the highest density case the electron density was

$$n_c = 2.1 \times 10^{18} \text{ m}^{-3}$$

and the electron temperature was

$$T_c = 17{,}400°\text{K} \ (1.5 \text{ eV}).$$

Substituting these values into Eq. (A-2) yielded an ion current to the walls of

$$I_{i_w} = 0.07 \text{ amp}$$

which was less than 2.2% of the electron current through the aperture (3.2 amp) as calculated by Eq. (11). Equation (A-2) can also be used to calculate the ion current through the baffle aperture if it is also assumed that the ions reach the aperture with the Bohm velocity. For this case the maximum observed ion current was calculated to be

$$I_{i_a} = 0.055 \text{ amp}$$

which was 2.54% of the electron current through the aperture. These examples represent the worst cases observed. The average ion currents were typically closer to 1% the aperture electron current.

APPENDIX B

COMPARISON OF CLASSICAL AND BOHM DIFFUSION COEFFICIENTS

In the course of the development of the baffle aperture model it was necessary to determine whether the classical or Bohm diffusion described electron flow through the aperture region more closely. For this reason an order of magnitude comparison of the theories with experimentally determined values of the diffusion coefficient was performed. The experimental diffusion coefficients were calculated by taking Eq. (25)

$$j_\perp = - D \left(\frac{e}{kT}\right) \left(ne \frac{dV}{dv} - \frac{dP}{dr}\right) \tag{B-1}$$

and writing it in the form,

$$D_{exp} \approx \frac{j_\perp}{\frac{\bar{n}e^2}{k\bar{T}} \frac{\Delta V}{\Delta r} - \frac{e}{k\bar{T}} \frac{\Delta P}{\Delta r}} \quad . \tag{B-2}$$

This equation computes an approximate average value of the diffusion coefficient through the aperture. The average density, $\bar{n}$, was computed according to Eq. (42) and the average temperature, $\bar{T}$, was computed from the equation,

$$\bar{T} = \frac{1}{2}\left(T_c + \frac{n_m T_m + n_p \varepsilon_p / k}{n_m + n_p}\right) \tag{B-3}$$

which roughly takes into account the presence of primary as well as Maxwellian electrons in the main discharge chamber. The distance over which the change in plasma properties occurs, Δr, was taken to be equal to the gap size* for all cases and was assumed to be the same for both

---

* The gap size was taken to be the distance from the downstream end of the cathode pole piece to the baffle plate for the radial field thruster.

the potential and density variations. The diffusion coefficients predicted by the Bohm diffusion theory were calculated from the equation,

$$D_B = \frac{k\bar{T}}{16eB_g} \tag{B-4}$$

where B_g is the magnetic flux density measured at the midpoint of the aperture gap. In addition the diffusion coefficients predicted by classical diffusion were calculated according to,

$$D_C = \frac{k\bar{T}m_e\nu}{e^2 B_g^2} \quad . \tag{B-5}$$

The collision frequency, ν, was calculated considering only electron-neutral and electron-ion collisions. The electron-neutral collision frequency, ν_{en}, was approximated from,[38]

$$\nu_{en} = n_n Q_n \bar{w}$$

where the neutral number density, n_n, can be determined from the theory developed by Wilbur.[39] The electron-neutral collision cross section was approximated from data given by Jahn[24] and the average electron velocity $\bar{w}$ was given by,

$$\bar{w} = \sqrt{\frac{8k\bar{T}}{\pi m_e}} \quad . \tag{B-6}$$

In addition the electron-ion collision frequency, ν_{ei}, was evaluated from the expression given by Holt and Haskel,[38]

$$\nu_{ei} = \frac{\bar{n} \ln \Lambda}{0.38\, \bar{T}^{3/2}} \, (10^{-6}) \tag{B-7}$$

where Λ is the non-dimensional plasma shielding distance which can be calculated from,[38]

$$\ln \Lambda = \ln \left[12.4 \times 10 \, \frac{\bar{T}^{3/2}}{\bar{n}^{1/2}} \right] \quad . \tag{B-8}$$

Table B-I shows the comparison of the diffusion coefficients calculated from the above equations for a number of cases covering a wide range of conditions. Clearly Bohm diffusion gives better results than the classical theory, the latter being typically at least an order of magnitude too small. In addition Table B-I lists the values of the electron cyclotron frequency, $\omega = eB/(2\pi m_e)$ and the collision frequency, ν, at these conditions. In all cases it is seen that the assumption $\omega/\nu >> 1$ is satisfied.

Table B-I

Diffusion Coefficients

Thruster Geometry	B_g [10^{-4}tesla]	ω [Hz]	ν [Hz]	D_{exp} [m^2/s]	D_B [m^2/s]	D_c [m^2/s]
Radial	16.7	4.6×10^7	1.4×10^6	200	100	8.0
Radial	92.7	2.5×10^8	8.4×10^6	180	120	1.0
Radial	58.4	1.6×10^8	1.5×10^6	43	37	0.9
Radial	42.1	1.2×10^8	2.8×10^6	53	37	2.2
Multipole	16.9	4.8×10^7	1.7×10^6	110	98	9.1
Multipole	27.0	7.5×10^7	2.4×10^6	26	66	5.3

APPENDIX C

MULTIPLE HOLLOW CATHODES

Plasma property measurements were made in a 15 cm multipole thruster equipped with two hollow cathodes in an effort to test the baffle aperture model. This thruster configuration is shown schematically in Fig. C-1. An assumption used in the derivation of the model was that the plasma in the cathode region would be azimuthally symmetric. This requirement was easily satisfied for the two cathode region geometries described earlier due to symmetry. However for the cylindrical shell geometry of this cathode discharge chamber and the azimuthally asymmetric location of the cathodes, this requirement is not readily satisfied. The first step to attempt to produce the desired symmetric plasma was to achieve operation at equal emission currents from both cathodes. Toward this end the cathodes were electrically isolated from the thruster body, as described in Appendix D, to facilitate measurement of the emission currents. Next, some method of controlling the current from each cathode was required. This control was effected by placing variable resistors in the leads to each cathode in the manner suggested by Fig. C-2, where the resistance in each lead was adjusted until the emission currents were equal. Control of the emission currents could also be achieved by adjustment of the cathode heater powers and neutral flow rates.[37] Unfortunately, regardless of the control scheme employed, the plasma in the cathode region was not azimuthally uniform even when both cathodes were emitting equally. The variation of density with azimuthal position (denoted by the angle θ from the right cathode) is shown for example in Fig. C-3. Clearly the electron density in the cathode region (circular symbols) is not uniform, in fact, it even falls

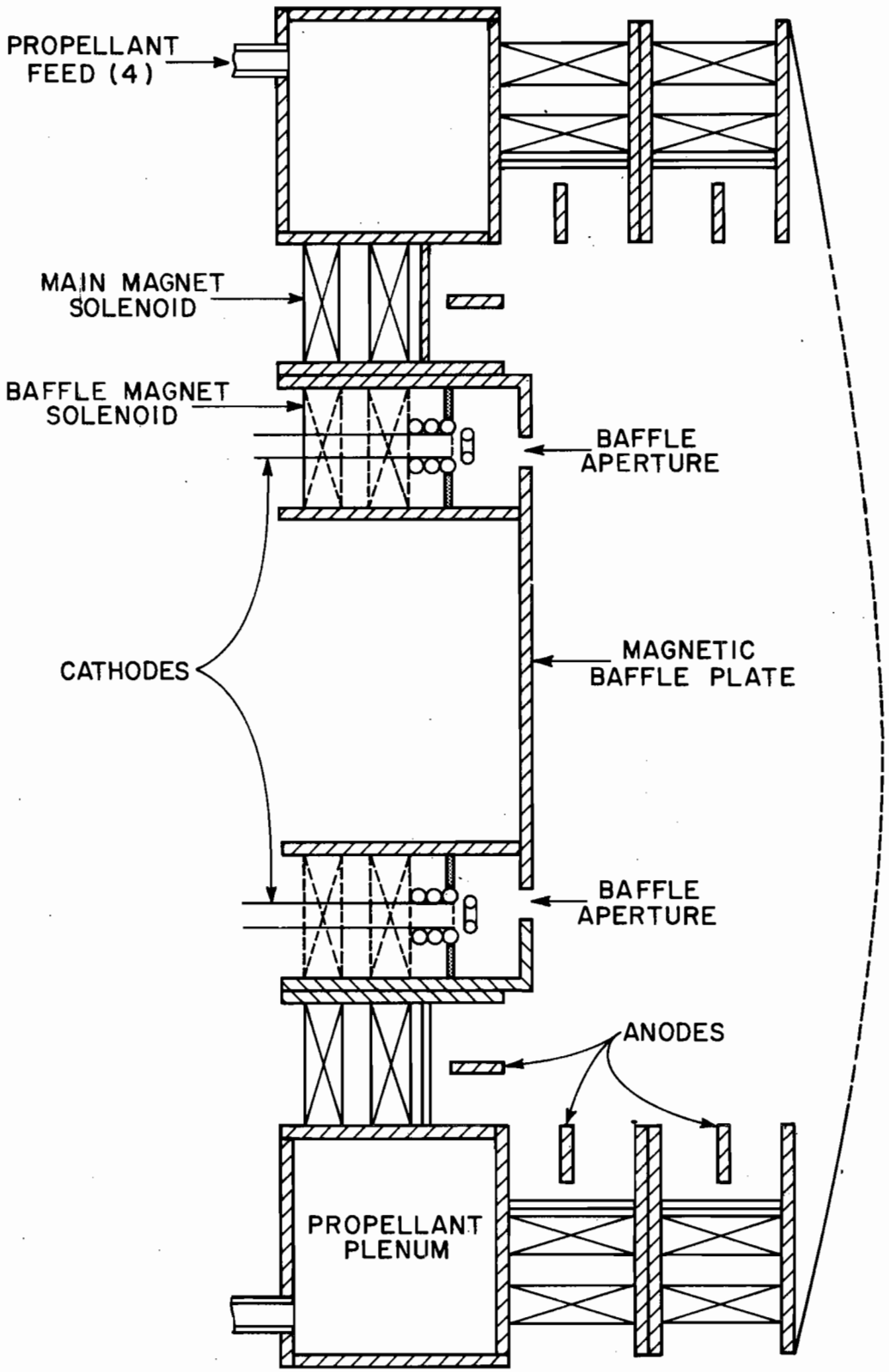

Fig. C-1 Multipole Thruster Equipped with Two Hollow Cathodes

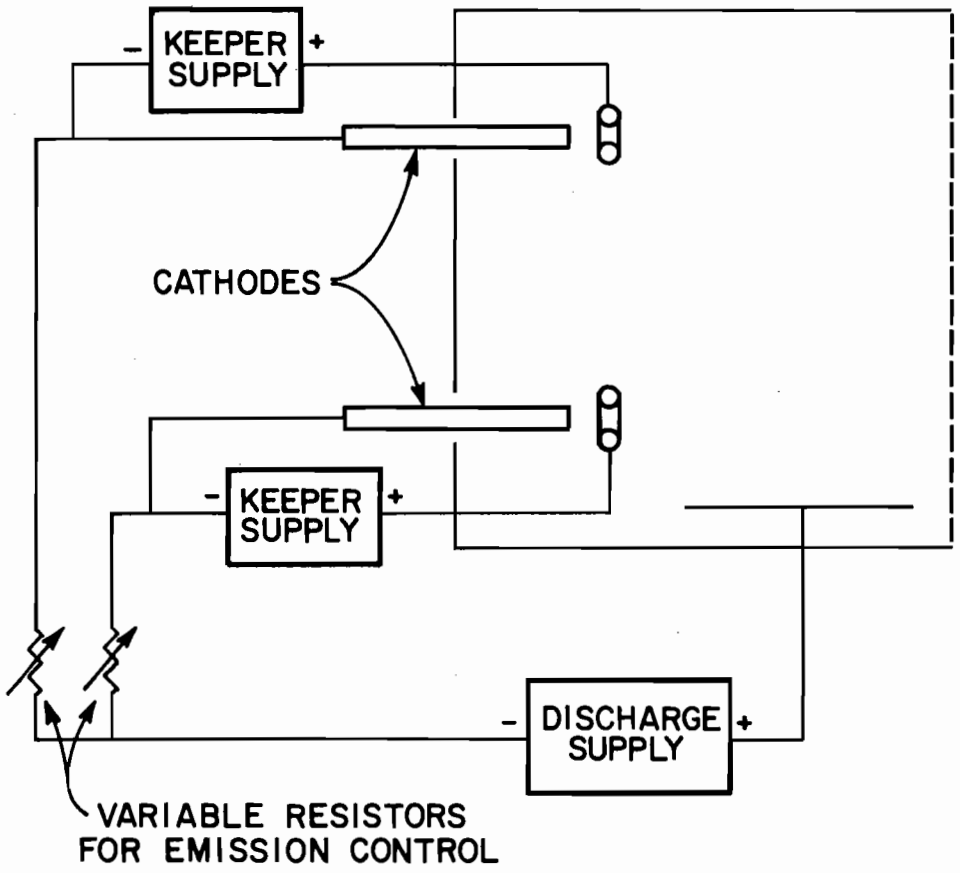

Fig. C-2 Location of Variable Resistors for Control of Relative Cathode Emission

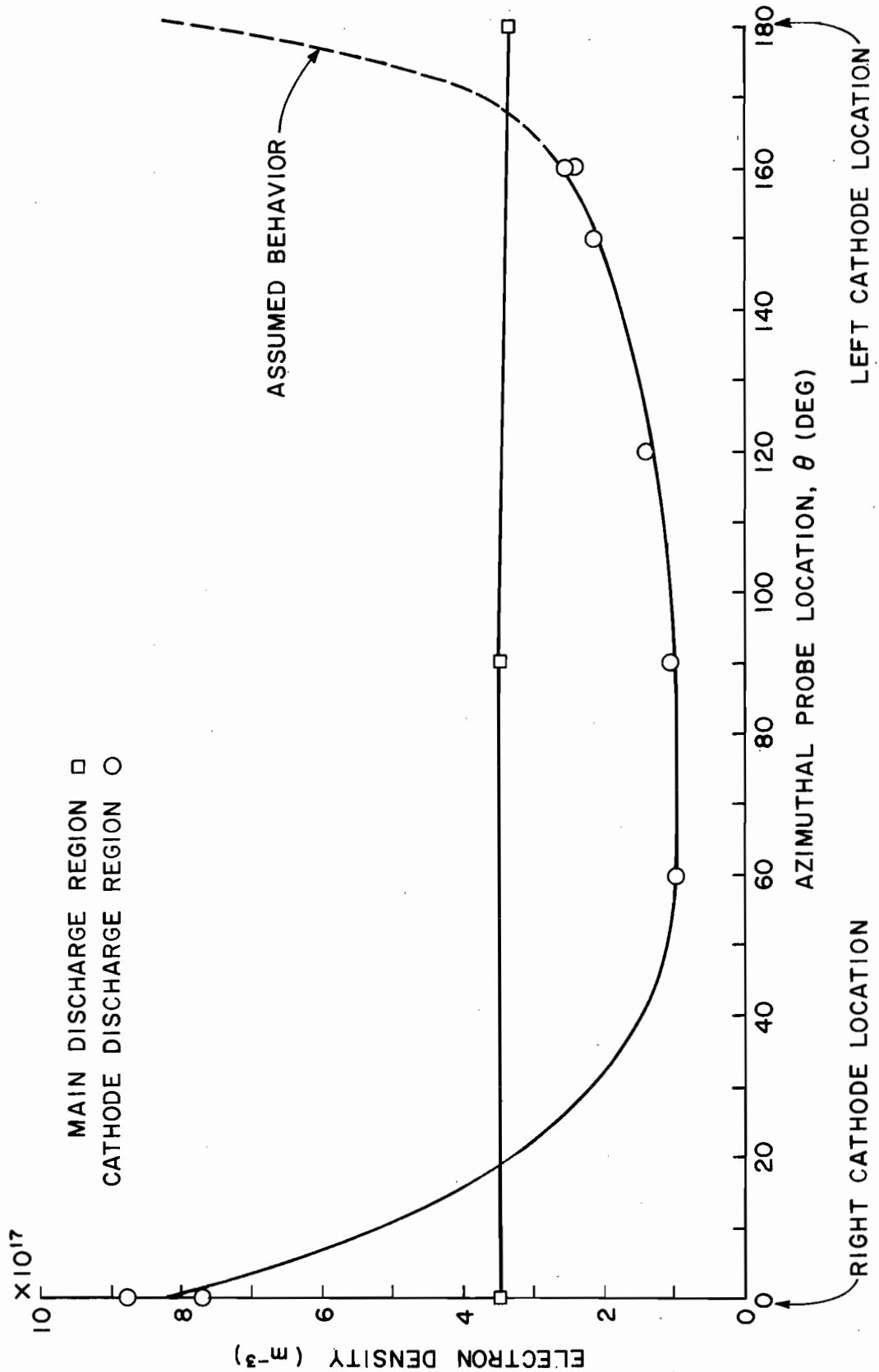

Fig. C-3 Axiumthal Plasma Variations

below the main discharge region density (square symbols) away from the cathodes. In spite of the asymmetry of the plasma in the cathode region the main discharge region plasma is seen to be quite uniform. Presumably, this is a consequence of the low magnetic field strength in this region which is characteristic of multipole thrusters. The thruster was operated over a wide range of conditions in several unsuccessful attempts to achieve a uniform cathode region plasma. Even reducing the aperture gap size from 5 mm to 2.5 mm did not facilitate a significant improvement in the uniformity. It is postulated that this azimuthal asymmetry is a result of the loss of ions to the cathode region walls in the azimuthal direction and the subsequent loss of electrons through the aperture. That is, the hollow cathodes act essentially as point plasma sources and the cathode region walls serve as distributed ion sinks. This combination could qualitatively produce the large azimuthal density gradients seen in Fig. C-3.

Finally, regardless of the exact mechanism involved, the proposed aperture region model could not be tested on this cathode configuration because of the cathode region plasma asymmetry. This asymmetry prohibits the one-dimensionalization of the diffusion equation. When plasma property gradients in both the azimuthal and normal directions are included in the analysis the equation for the current density through the aperture ($j_\perp$) determined from Eqs. (18) and (19) becomes,

$$j_\perp = -\frac{\nu e}{m_e(\nu^2 + \omega^2)}(ne\nabla_\perp V - \nabla_\perp P) + \frac{\omega^2}{B(\nu^2 + \omega^2)}(ne\nabla_\theta V - \nabla_\theta P) \tag{C-1}$$

and the current density in the azimuthal direction is given by,

$$j_\theta = -\frac{\nu e}{m_e(\nu^2 + \omega^2)}(ne\nabla_\theta V - \nabla_\theta P) - \frac{\omega^2}{B(\nu^2 + \omega^2)}(ne\nabla_\perp V - \nabla_\perp P) . \tag{C-2}$$

The presence of the azimuthal plasma property gradients in Eq. (C-1) prohibits the use of the simplifications applied in Chapter III to the one-dimensional analysis. Consequently, plasma property measurements to be used as inputs to these equations could not be limited to one point from the main discharge region and one from the cathode region. Further, requiring plasma data to be used as inputs to the model from more than two locations would make the model prohibitively difficult to use as a design tool.

In addition, it is pointed out that if the Bohm diffusion coefficient is incorporated into Eq. (C-1) in the same manner as before and neglecting ν^2 relative to ω^2 Eq. (C-1) becomes,

$$j_\perp = -\frac{1}{16B}\left(ne\nabla_\perp V - \nabla_\perp P\right) + \frac{1}{B}\left(ne\nabla_\theta V - \nabla_\theta P\right) \quad . \qquad (C\text{-}3)$$

This equation indicates that even small azimuthal gradients (relative to the gradients in the normal direction) can have a significant effect on the current through the aperture.

APPENDIX D

ELECTRICAL ISOLATION OF CATHODE

In order to measure the emission current from a hollow cathode in an operating ion thruster it is necessary to isolate electrically from the thruster body. In this study the cathode was isolated from the body with boron nitride insulators and electrical connections were made in accordance with Fig. D-1. These connections included the addition of a lead from the negative side of the anode power supply to the thruster body to supply electrons to neutralize the ions reaching the body. The location of the ammeter shown in this figure allows it to measure only the net cathode emission current, I_E, (i.e., the current emitted by the cathode and not subsequently collected by the keeper). The extension to additional cathodes is straightforward, where additional keeper, vaporizer, and cathode heater power supplies are required for each additional cathode.

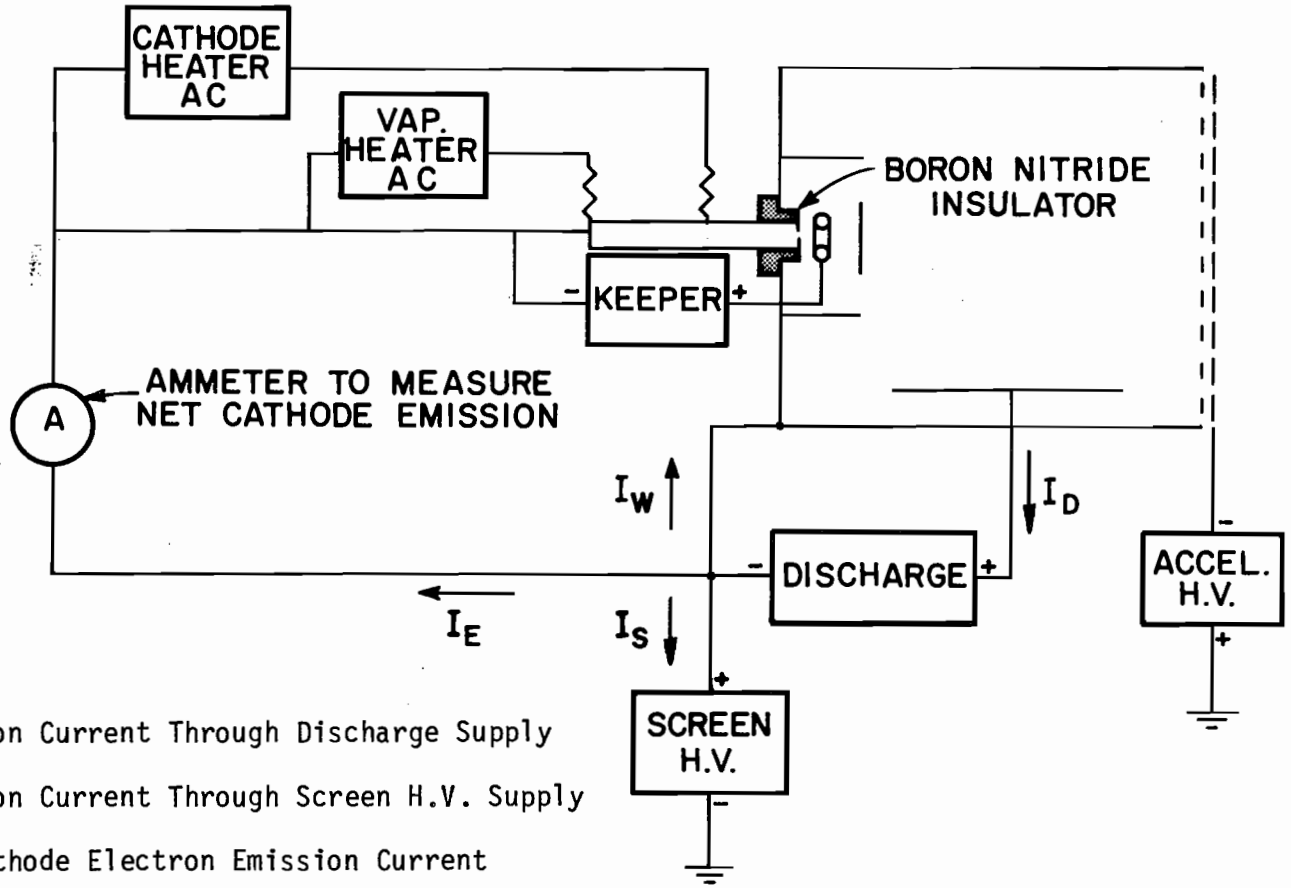

I_D = Electron Current Through Discharge Supply

I_S = Electron Current Through Screen H.V. Supply

I_E = Net Cathode Electron Emission Current

I_w = Electron Current to Thruster Body

Fig. D-1 Electrically Isolated Cathode Circuit Diagram

APPENDIX E

APERTURE REGION MAGNETIC FIELD MEASUREMENTS

In order to test the validity of Eq. (46) it was necessary to determine the values of the integral on the left-hand side of this equation by directly measuring the area through which the current flows and the magnetic field variation through the aperture. A closeup drawing of the radial field's cathode pole piece baffle aperture region is given in Fig. E-1a. For this particular geometry it is assumed the electron current flows through increasingly larger diameter right circular cylinders as it traverses the baffle aperture region as suggested by the dashed lines in Fig. E-1a. In reality the current flow is normal to the magnetic field vectors[17] but the error introduced by using the area variation of Fig. E-1a is believed to be negligible since the magnetic field vectors through the aperture point primarily in the axial direction. Figure E-1b shows the normalized area variation through the aperture as determined from Fig. E-1a. The area was normalized according to the formula,

$$A^* = A/A_g \ . \tag{E-1}$$

In addition it was found convenient for data analysis purposes to normalize the magnetic field strength and radial position according to the formulas,

$$B^* = B/G_g \tag{E-2}$$

and

$$r^* = r/r_g \tag{E-3}$$

where the stars indicate dimensionless quantities and the subscript "g"

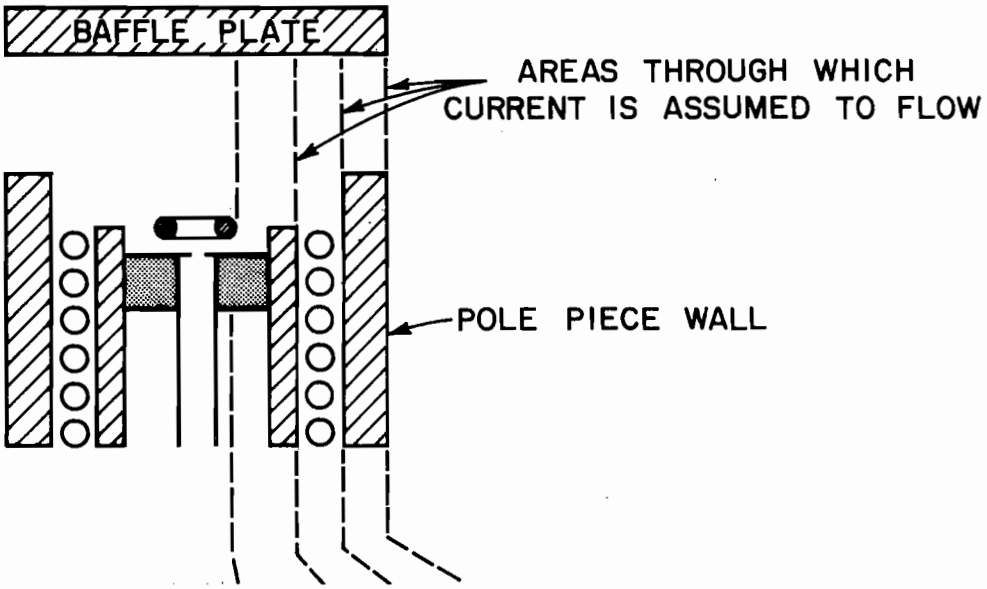

Fig. E-1a Radial Field Cathode Pole Piece Baffle Aperture Region Showing Area Through which the Electron Current is Assumed to Flow

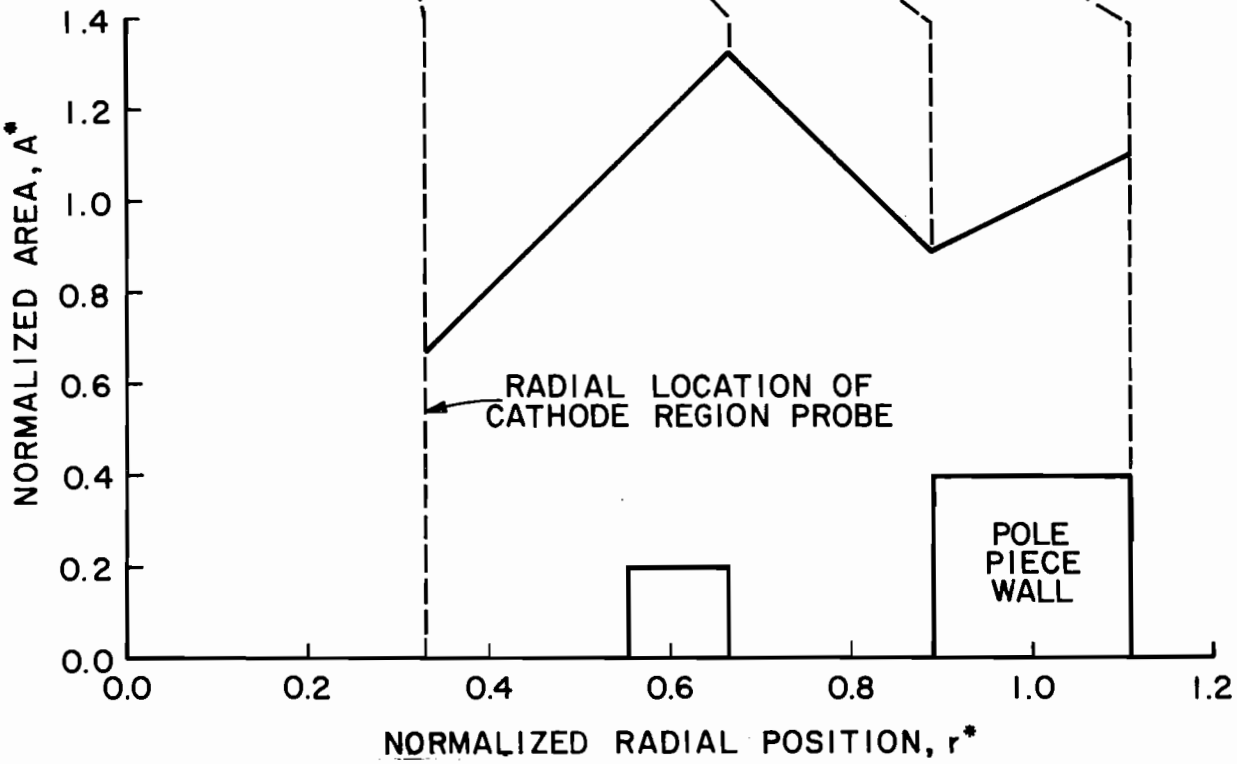

Fig. E-1b Example of Normalized Area Variation Through the Aperture Determined According to Fig. E-1a.

refers to quantities pertaining to the center of the aperture gap. The magnetic field variation through the aperture was measured at ten radial loations with a two axis gauss meter. This was done for each gap size and current setting of the electromagnets tested because the shape as well as the strength of the magnetic field in this region depended on the values of these parameters. A typical example of the magnetic field variation normalized with the magnetic field strength in the gap (B_g) is given as a function of the non-dimensionalized radial position (r/r_g) in Fig. E-2. If at each radial position the value of the magnetic field strength (B^*) is divided by the area (A^*) from Figs. E-2 and E-1b respectively, the result is the variation of (B^*/A^*) through the aperture given in Fig. E-3. Now integration of this curve will yield the value of the non-dimensionalized integral $\int B^*/A^* \, dr^*$. The distance over which this integration is performed is of primary importance. The proper value of the integral is determined by integrating over the distance between the radial location of the cathode region probe and the critical magnetic field line. Using Eqs. (E-1), (E-2) and (E-3) the dimensional value of the integral can be recovered from,

$$\int \frac{B}{A} \, dr = \frac{B_g r_g}{A_g} \int \frac{B^*}{A^*} \, dr \quad . \qquad \text{(E-4}$$

As mentioned previously, this was done for each different electromagnet current setting and aperture area. The same procedure was followed for the determination of the integral, $\int \frac{B}{A} \, dz$, for the multipole thruster configuration. It was noted in this case, however, that the field shape through the aperture was independent of the current through the main electromagnets. This is because the baffle aperture

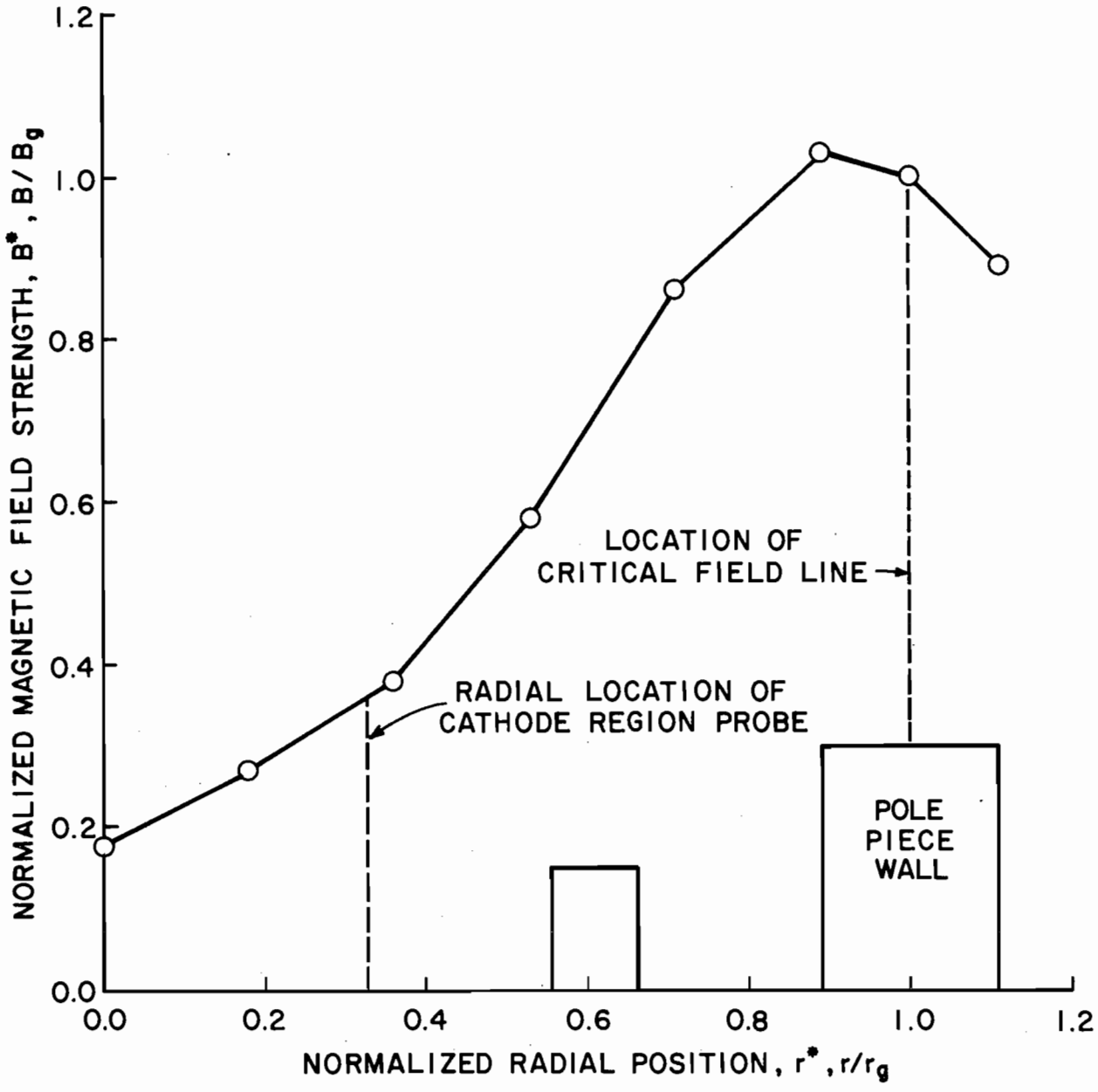

Fig. E-2 Example of Normalized Magnetic Field Strength Variation Through the Aperture

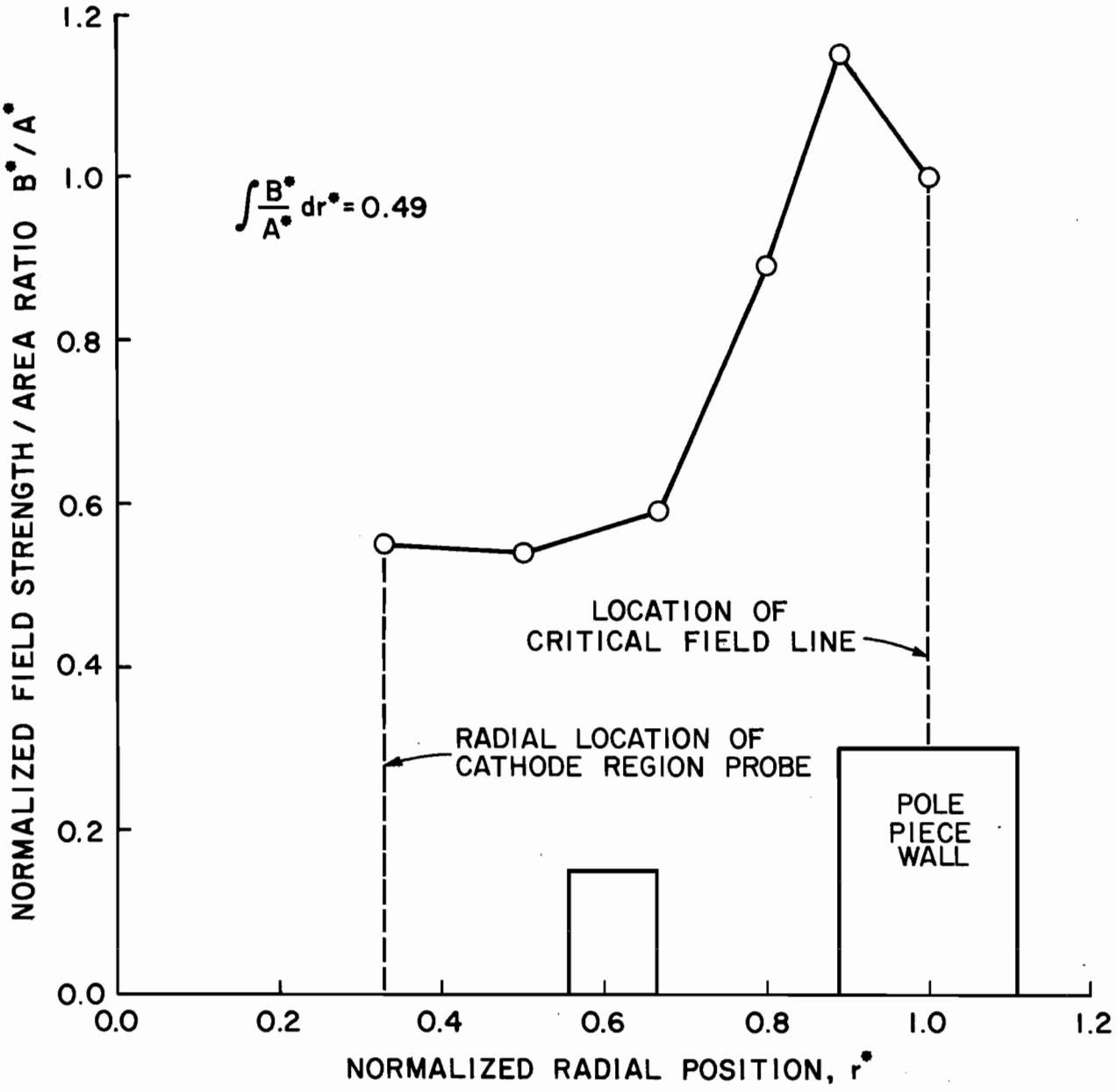

Fig. E-3 Example of Variation of the Ratio B*/A* Through the Aperture as Determined from Fig. E-1b and E-2

pole piece was not part of the main discharge region's magnetic circuit. In addition, evaluation of the integral was performed over the distance between the two probes due to the vagueness of the location of the critical magnetic field line in this thruster.